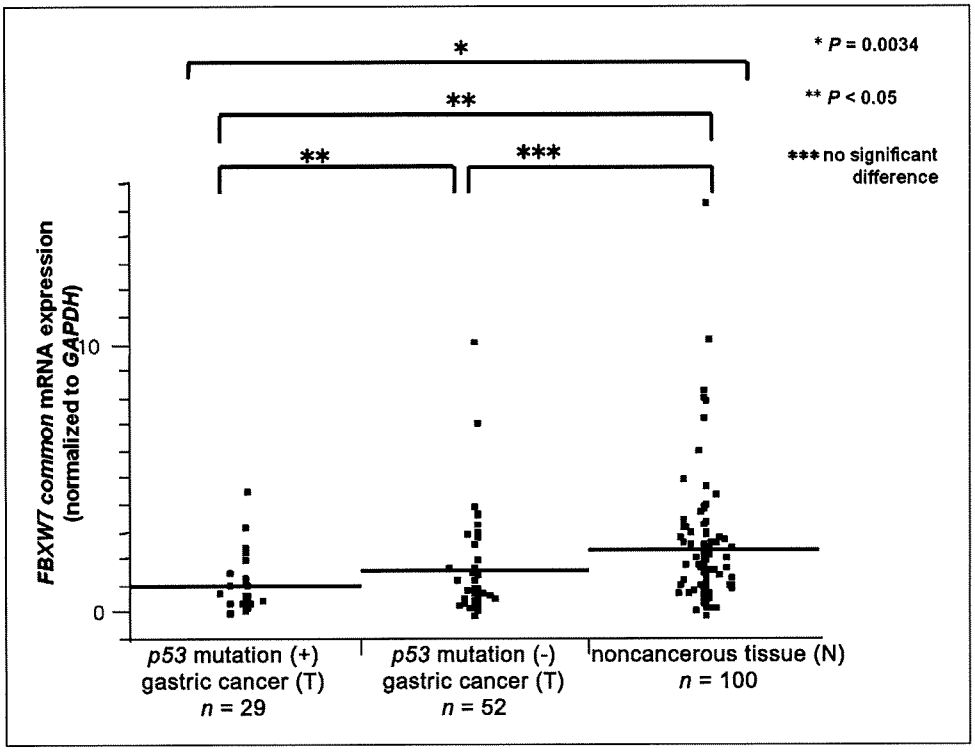

Figure 3. Relationship between *FBXW7* mRNA expression and *p53* mutation. Gastric cancer patients were divided into two groups based on the presence or absence of the *p53* mutation. The two groups were the *p53* mutation (+) gastric cancer group (n = 29) and the *p53* mutation (–) gastric cancer group (n = 52). *FBXW7* expression levels in *p53* mutation (+) patients were lower than in the other groups. *Horizontal lines*, mean expression value of each group. The statistical analysis for comparisons was done in the order of ANOVA and Tukey's test.

Third, chromosome 4q contains the *FBXW7* gene. Approximately 30% of the gene is deleted in certain carcinomas, such as esophageal and gastric cancers. In particular, inactivation of tumor suppressor genes by the chromosome 4q deletion may be an important factor in colon carcinogenesis (22–24).

The reduction of *FBXW7* expression is associated with the dysregulation of cyclin E and c-Myc, positive regulators of the cell cycle (2, 18, 25, 26). c-Myc is associated with cell growth and is recognized as an important factor in control of the G_1 (G_0) to S-phase transition (1, 6, 27, 28). Cyclin E expression is enhanced in various types of cancer, where it regulates cell cycle progression via Rb phosphorylation and contributes to genome instability (19, 29). Consistent with previously published reports, we showed that protein expression of c-Myc and cyclin E is enhanced when *FBXW7* is suppressed in a gastric cancer cell line (Fig. 4). Immunohistochemical analysis of FBXW7 in clinical gastric cancer tissues revealed enhanced expression of Myc and cyclin E in FBXW7 low expression tissues (Supplementary Fig. S7*A*). Conversely, Myc and

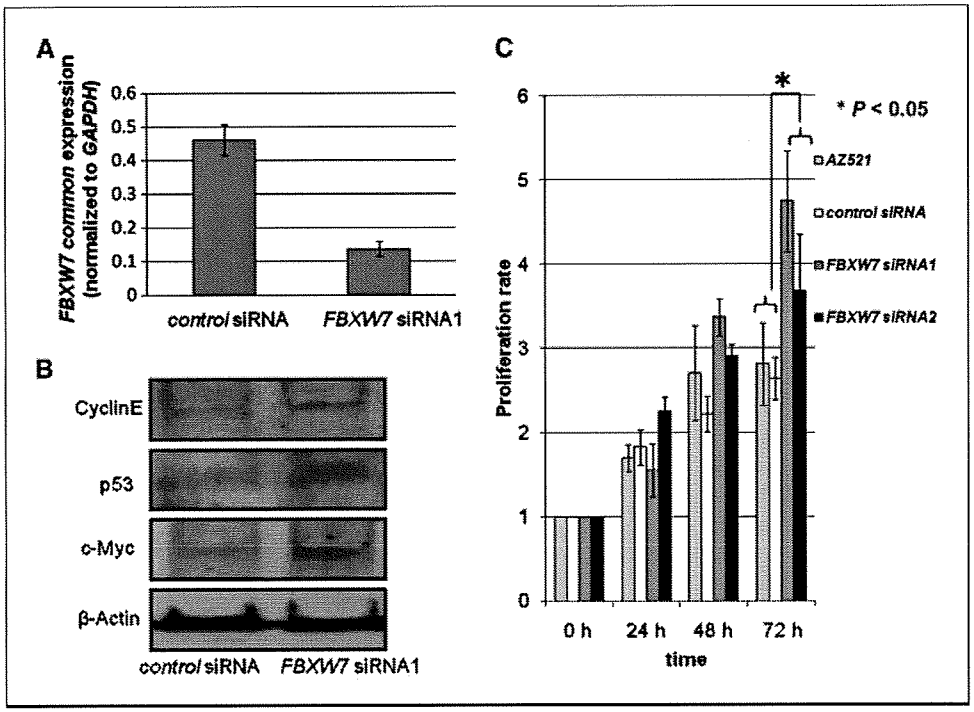

Figure 4. Proliferation assay with RNA interference of *FBXW7* in the AZ521 gastric cancer cell line. *A*, reduced *FBXW7* expression was confirmed by quantitative reverse transcription-PCR analyses in *FBXW7* siRNA1 cells compared with control siRNA. *FBXW7* expressions were normalized by *GAPDH* expression. Mean ± SD. *B*, Western blot analysis of c-Myc, cyclin E, and p53 in *FBXW7* siRNA cells and control siRNA cells. These proteins were normalized to the level of β-actin. *C*, 3-(4,5-dimethylthiazol-2-yl)-2,5-diphenyltetrazolium bromide assay. The proliferation rate of *FBXW7* siRNA (1 and 2) cells was enhanced over that of control siRNA and parent AZ521 cells. Mean ± SD.

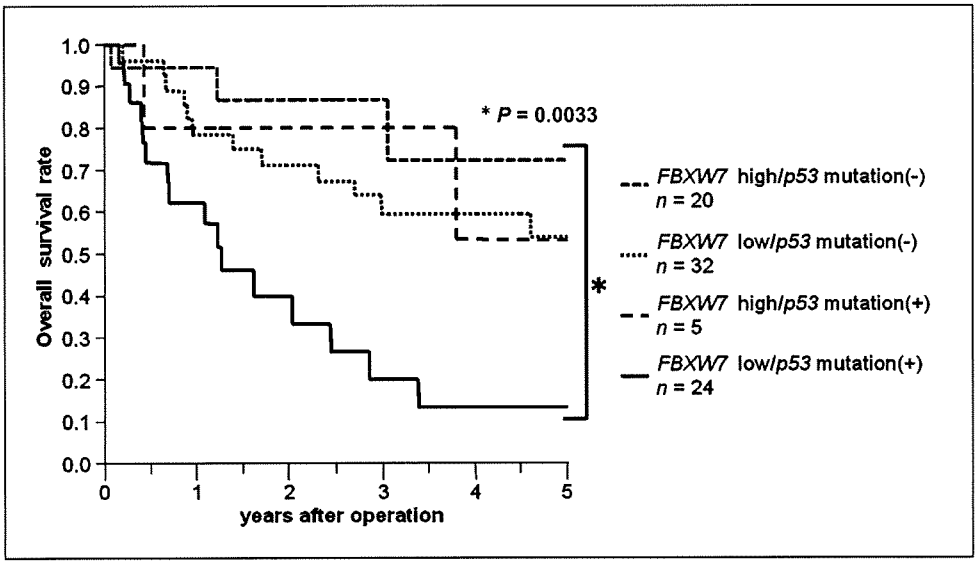

Figure 5. Kaplan-Meier overall survival curves of gastric cancer patients based on *FBXW7* mRNA expression and *p53* mutation. The survival rate for patients in the low *FBXW7* expression and *p53* mutation (+) group was significantly lower than that for patients in the other three groups ($P < 0.05$): high *FBXW7* expression and *p53* mutation (−; $n = 20$), high *FBXW7* expression and *p53* mutation (+; $n = 5$), low *FBXW7* expression and *p53* mutation (−; $n = 32$), and low *FBXW7* expression and *p53* mutation (+; $n = 24$).

cyclin E expression levels were suppressed in tissues in which FBXW7 was overexpressed (Supplementary Fig. S7*B*), confirming the relationship between FBXW7 and target proteins in clinical gastric cancer tissues.

In addition, c-Myc accumulation induces p53-dependent apoptosis via MDM2 degradation (6, 30, 31). The inactivation of both *FBXW7* and *p53* promotes c-Myc accumulation and inhibits p53-dependent apoptosis by MDM2 activation. It probably means that the proliferation rate was increased in these cells.

The low *FBXW7* expression group of gastric cancer patients showed progression of clinicopathologic factors and poor prognosis. All 4 cases of liver metastasis (100%, 4 of 4), 16 cases of peritoneal dissemination (94%, 16 of 17), and 24 cases of venous invasion (86%, 24 of 28) were classified as members of the *FBXW7* low expression group (Table 1). Unfortunately, a significant correlation was not observed between the incidence of liver metastasis and *FBXW7* expression because of an insufficient number of cases. However, other clinicopathologic findings indicated that FBXW7 contributes to hematogenous metastasis besides lymph node metastasis and peritoneal dissemination.

FBXW7 is a tumor suppressor. Considering tumor dormancy as one way to conquer malignancies, the introduction of FBXW7 may facilitate "tumor dormancy therapy." Moreover, it was found that Myc inhibition triggers rapid regression of incipient and established lung tumors *in vivo* (32). Therefore, Myc degradation by FBXW7 may not only induce a state of tumor dormancy but also could have an antitumor effect.

As in a previous *in vivo* study, the simultaneous disruption of two cell cycle checkpoint genes, *p53* and *FBXW7*, shortened the survival of mice with thymic lymphomas (6). It is notable that, even in the *FBXW7* low expression group, the 5-year survival rate of *p53* mutation (−) cases is 53%, but we found that it was 14% in the *FBXW7* low expression/*p53* mutation (+) group of clinical gastric cancer patients (Fig. 5). Both *p53* and *FBXW7* act to brake the cell cycle. Therefore, simultaneous disruption of these genes led to poor prognosis in clinical gastric cancer in comparison with inactivation of *p53* or *FBXW7* alone. Although p53 reportedly regulates *FBXW7* expression, other mechanisms may be present. In the current study, most cases of *p53* mutation (+) gastric cancer were in the low *FBXW7* group and had poor prognosis (83%, 24 of 29). However, a few cases of *p53* mutation (+) gastric cancer were in the high *FBXW7* expression group (17%, 5 of 29) and had good prognosis in comparison with the *p53* mutation (+)/low *FBXW7* group. There were a few cancer cases with higher *FBXW7* expression that was not regulated by p53. Therefore, the prognosis of *p53* mutation (+) cases is not identical to that of *p53* mutation (+)/*FBXW7* low cases.

These results show that the status of *FBXW7* and *p53* is critical for prognosis determination in gastric cancer patients. This report is the first confirmation of the experimental mice data using clinical gastric cancer samples.

In conclusion, *FBXW7* has recently attracted attention as a tumor suppressor gene that reduces important oncoproteins and related carcinogenesis and cell cycle progression. There are previous reports of *in vitro* and *in vivo* studies showing that p53 controls *FBXW7* expression and that *FBXW7* inactivation contributes to poor prognosis via genome instability and cell cycle progression. However, these findings had not been shown in clinical cancer samples. We have clarified that gastric cancer patients with inactivation of *FBXW7* and *p53* have a poorer prognosis.

Disclosure of Potential Conflicts of Interest

No potential conflicts of interest were disclosed.

Acknowledgments

Received 8/5/08; revised 2/2/09; accepted 2/25/09; published OnlineFirst 4/14/09.

Grant support: CREST, Japan Science and Technology Agency; Japan Society for the Promotion of Science Grant-in-Aid for Scientific Research grants 17109013, 18659384, 18390367, 18590333, 18015039, 19591509, 19390336, 20390360, 20591547, 20790961, 20659209, and 20790960; The Ministry of Education, Culture, Sports, Science and Technology Grant-in-Aid for Scientific Research on Priority Areas grant 18015039; Third-Term Comprehensive 10-Year Strategy for Cancer Control grant 16271201; New Energy and Industrial Technology Development Organization Technological Development for Chromosome Analysis; The Ministry of Education, Culture, Sports, Science and Technology of Japan for Scientific Research on Priority Areas, Cancer Translational Research Project; and Grant of Clinical Research Foundation 2008-2010.

The costs of publication of this article were defrayed in part by the payment of page charges. This article must therefore be hereby marked *advertisement* in accordance with 18 U.S.C. Section 1734 solely to indicate this fact.

We thank T. Shimooka, K. Ogata, M. Kasagi, Y. Nakagawa, and T. Kawano for technical assistance.

References

1. Nakayama KI, Nakayama K. Ubiquitin ligases: cell-cycle control and cancer. Nat Rev Cancer 2006;6:369–81.
2. Welcker M, Clurman BE. FBW7 ubiquitin ligase: a tumour suppressor at the crossroads of cell division, growth and differentiation. Nat Rev Cancer 2008;8:83–93.
3. Mao JH, Perez-Losada J, Wu D, et al. Fbxw7/Cdc4 is a p53-dependent, haploinsufficient tumour suppressor gene. Nature 2004;432:775–9.
4. Akhoondi S, Sun D, von der Lehr N, et al. FBXW7/hCDC4 is a general tumor suppressor in human cancer. Cancer Res 2007;67:9006–12.
5. Matsumoto A, Onoyama I, Nakayama KI. Expression of mouse Fbxw7 isoforms is regulated in a cell cycle- or p53-dependent manner. Biochem Biophys Res Commun 2006;350:114–9.
6. Onoyama I, Tsunematsu R, Matsumoto A, et al. Conditional inactivation of Fbxw7 impairs cell-cycle exit during T cell differentiation and results in lymphomatogenesis. J Exp Med 2007;204:2875–88.
7. Matsuoka S, Oike Y, Onoyama I, et al. Fbxw7 acts as a critical fail-safe against premature loss of hematopoietic stem cells and development of T-ALL. Genes Dev 2008;22:986–91.
8. Kimura T, Gotoh M, Nakamura Y, Arakawa H. hCDC4b, a regulator of cyclin E, as a direct transcriptional target of p53. Cancer Sci 2003;94:431–6.
9. Nakayama KI, Nakayama K. Regulation of the cell cycle by SCF-type ubiquitin ligases. Semin Cell Dev Biol 2005;16:323–33.
10. Yan T, Wunder JS, Gokgoz N, Seto KK, Bell RS, Andrulis IL. hCDC4 variation in osteosarcoma. Cancer Genet Cytogenet 2006;169:138–42.
11. Hagedorn M, Delugin M, Abraldes I, et al. FBXW7/hCDC4 controls glioma cell proliferation *in vitro* and is a prognostic marker for survival in glioblastoma patients. Cell Div 2007;2:9.
12. Bredel M, Bredel C, Juric D, et al. Functional network analysis reveals extended gliomagenesis pathway maps and three novel MYC-interacting genes in human gliomas. Cancer Res 2005;65:8679–89.
13. Lee JW, Soung YH, Kim HJ, et al. Mutational analysis of the hCDC4 gene in gastric carcinomas. Eur J Cancer 2006;42:2369–73.
14. Enders GH. Cyclins in breast cancer: too much of a good thing. Breast Cancer Res 2002;4:145–7.
15. Ogawa K, Utsunomiya T, Mimori K, et al. Clinical significance of human kallikrein gene 6 messenger RNA expression in colorectal cancer. Clin Cancer Res 2005;11:2889–93.
16. Ieta K, Ojima E, Tanaka F, et al. Identification of overexpressed genes in hepatocellular carcinoma, with special reference to ubiquitin-conjugating enzyme E2C gene expression. Int J Cancer 2007;121:33–8.
17. Ieta K, Tanaka F, Utsunomiya T, Kuwano H, Mori M. CEACAM6 gene expression in intrahepatic cholangiocarcinoma. Br J Cancer 2006;95:532–40.
18. Welcker M, Orian A, Grim JE, Eisenman RN, Clurman BE. A nucleolar isoform of the Fbw7 ubiquitin ligase regulates c-Myc and cell size. Curr Biol 2004;14:1852–7.
19. Minella AC, Grim JE, Welcker M, Clurman BE. p53 and SCF(Fbw7) cooperatively restrain cyclin E-associated genome instability. Oncogene 2007;26:6948–53.
20. Malyukova A, Dohda T, von der Lehr N, et al. The tumor suppressor gene hCDC4 is frequently mutated in human T-cell acute lymphoblastic leukemia with functional consequences for Notch signaling. Cancer Res 2007;67:5611–6.
21. Tan Y, Sangfelt O, Spruck C. The Fbxw7/hCdc4 tumor suppressor in human cancer. Cancer Lett 2008;271:1–12.
22. Sterian A, Kan T, Berki AT, et al. Mutational and LOH analyses of the chromosome 4q region in esophageal adenocarcinoma. Oncology 2006;70:168–72.
23. Sundqvist A, Bengoechea-Alonso MT, Ye X, et al. Control of lipid metabolism by phosphorylation-dependent degradation of the SREBP family of transcription factors by SCF(Fbw7). Cell Metab 2005;1:379–91.
24. Takada H, Imoto I, Tsuda H, et al. Screening of DNA copy-number aberrations in gastric cancer cell lines by array-based comparative genomic hybridization. Cancer Sci 2005;96:100–10.
25. Welcker M, Orian A, Jin J, et al. The Fbw7 tumor suppressor regulates glycogen synthase kinase 3 phosphorylation-dependent c-Myc protein degradation. Proc Natl Acad Sci U S A 2004;101:9085–90.
26. Welcker M, Singer J, Loeb KR, et al. Multisite phosphorylation by Cdk2 and GSK3 controls cyclin E degradation. Mol Cell 2003;12:381–92.
27. Spencer CA, Groudine M. Control of c-myc regulation in normal and neoplastic cells. Adv Cancer Res 1991;56:1–48.
28. Onoyama I. Cyclin E and c-Myc degradation by SCF(Fbxw7). Tanpakushitsu Kakusan Koso 2006;51:1382–5.
29. Ji P, Zhu L. Using kinetic studies to uncover new Rb functions in inhibiting cell cycle progression. Cell Cycle 2005;4:373–5.
30. Zindy F, Eischen CM, Randle DH, et al. Myc signaling via the ARF tumor suppressor regulates p53-dependent apoptosis and immortalization. Genes Dev 1998;12:2424–33.
31. Pelengaris S, Khan M. The many faces of c-MYC. Arch Biochem Biophys 2003;416:129–36.
32. Soucek L, Whitfield J, Martins CP, et al. Modelling Myc inhibition as a cancer therapy. Nature 2008;455:679–83.

Int. J. Cancer: **125,** 2270–2280 (2009)

The reduction of cell death and proliferation by $p27^{Kip1}$ minimizes DNA damage in an experimental model of genotoxicity

Isidora Ranchal[1#], Raúl González[1#], Rosario I. Bello[1], Gustavo Ferrín[1#], Ana B. Hidalgo[1], Clara I. Linares[1], Patricia Aguilar-Melero[1], Sandra González-Rubio[1], Pilar Barrera[1#], Trinidad Marchal[2#], Keiichi I. Nakayama[3], Manuel de la Mata[1#] and Jordi Muntané[1#*]

[1]*Liver Research Unit, Reina Sofia University Hospital, Córdoba, Spain*
[2]*Department of Pathology, Reina Sofia University Hospital, Córdoba, Spain*
[3]*Department of Molecular and Cellular Biology, Medical Institute of Bioregulation, Kyushu, Japan*
[#]*Centro de Investigación Biomédica en Red de Enfermedades Hepáticas y Digestivas (CIBEREHD o Ciberehd)*

Hepatocellular carcinoma (HCC) is the fifth most commonly occurring cancer worldwide. The expression of p27 has been related to reduced severity of tumor grade and recurrence of HCC. The study assessed the role of p27 on the cell proliferation and death, and DNA mutagenesis in experimental genotoxicity induced by aflatoxin B1 (AFB_1) in cultured hepatocytes obtained from control and $p27^{Kip1}$ deficient mice. The overexpression of p27 was assessed with wild type $p27^{Kip1}$ expression vector in HepG2 cells. The expression of p27, p21 and p53 was assessed in well and poorly-differentiated liver tumors. DNA damage and cell death induced by AFB_1 were related to a reduction of p27 and p21 expression in cultured hepatocytes. AFB_1-induced nuclear phosphorylated (Ser 10) p27 degradation was related to a rise of nuclear KIST, Rsk-1 and Rsk-2 expression and cytoplasm phosphorylated (Thr 198) p27 expression. The overexpression of p27 reduced cell proliferation, cell death and DNA damage in AFB_1-treated hepatocytes. The enhanced survival of patients with well differentiated compared to poorly-differentiated tumors was related to high expression of p27, p21 and p53 in liver sections. The study showed that the p27 reduced cell proliferation and death, as well as the accumulation of DNA damage in hepatocarcinogenesis.
© 2009 UICC

Key words: HCC; AFB_1; cell cycle; p27; p21

Hepatocellular carcinoma (HCC) is a major health problem, being the sixth most common cancer worldwide with 626,000 new cases in 2002, and the third greatest cause of cancer mortality.[1,2] The distribution pattern of HCC shows geographical variation and its pathogenesis is multifactorial.[3] Environmental, infectious, nutritional, metabolic and endocrine factors contribute directly or indirectly to hepatocarcinogenesis.[3] Although some advances have been achieved in the diagnosis and treatment of HCC, the long-term outcome for patients with HCC is still very poor. The prognosis for HCC depends mainly on the clinico-pathological characteristics regarding invasion and metastasis.[4] Surgery, in the form of either hepatic resection or orthotopic liver transplantation, is the only potentially curative treatment.[5,6] HCC recurrence rates at 1, 2, 3, 4 and 5 years were 30, 52, 62, 69 and 79%, respectively,[7] and 5 years survival rates of 30–50%.[8] The molecular changes correlated with recurrence or metastasis of HCC would be useful to screen patients with high risk of recurrence.[4,9,10] Although many biomarkers have been tried, such as α-fetoprotein (AFP) mRNA, circulating VEGF and PD-ECGF, human macrophage metalloelastase gene,[11] p27,[12] p53 mutation,[9] p73 expression,[13] telomerase activity,[14] *etc.*, a routine biomarker for prediction of metastasis and recurrence is not yet available.

Aflatoxin B_1 (AFB_1) are naturally occurring mycotoxins elaborated by *Aspergillus flavus* and *Aspergillus parasiticus* that grow readily on foodstuffs stored in damp conditions like mouldy rice, hundredth wheat, barley, *etc.* The adverse health effects associated with AFB_1 exposure range from acute liver toxicities to liver cancer in humans.[15] AFB_1 is metabolized to a reactive electrophile intermediated, AFB_1-*exo*-8,9-epoxide by hepatic cytochrome P450-family member, CYP1A2 and CYP3A4, which has been shown to bind and damage DNA.[16] Different reports have showed that a G to T transversion of the third nucleotide in codon 249 of the p53 gene (249^{ser}),[17,18] and ras and myc activation[19] are associated with AFB_1-induced HCC.

The maintenance of cell cycle checkpoints is essential for the maintenance of normal cell growth, and protects the cell from DNA damage and malignancy. The different cell cycle phases are controlled by cyclins acting as positive regulatory subunit in the cyclin/Cyclin-dependent kinase (CDK) complexes, which are expressed periodically during the cell cycle.[20] CDKs are controlled by phosphorylation that either stimulates or represses catalytic activity.[21] CDK inhibitors (CKIs) interact with distinct cyclin/CDK complexes, thereby interfering with their activity.[22] CKIs inhibit CDK4 and CDK6 ($p16^{Ink4a}$, $p15^{Ink4b}$, $p18^{Ink4c}$ and $p19^{Ink4}$) or CDK2 ($p21^{Cip1}$, $p27^{Kip1}$ and $p57^{Kip2}$) families. CKIs induce cell-cycle arrest in response to anti-proliferative signals, including contact inhibition and serum deprivation, TGF-β, myogenic, myeloid and neuronal differentiation, and DNA-damage checkpoints.[20,23] $p27^{Kip1}$ (p27) was originally identified as a inhibitor of G1 cyclin/CDK complex levels,[24] increases in response to differentiation signals,[25] and it is thought to have an important role in cancer.[26] p27 is frequently overexpressed in HCC, which is related to longer disease-free survival.[27] The underexpression of p27 has been associated with more severe tumor grade and recurrence, as well as a negative prognostic marker in HCC.[28–30]

Being associated with one of the central interfaces that control the cell cycle, p27 is itself highly regulated. The differential expression of the gene and the protein as well as several distinct post-translational modifications have been uncovered as mechanisms that control the activity of p27.[31] The aim of the present study was to determine if the overexpression or deficiency of p27, as well as post-traductional modifications are able to modulate cell death and DNA mutagenesis, as well as the expression of p21 and p53 in an experimental model of genotoxicity by AFB_1.

Material and methods

Preparation of primary mice hepatocytes and cell culture

Male Wild-type (C57BL/6J) and p27 knockout (B6.129S4-*Cdkn1b*^{tm1Mlf}/*J*) mice of 10 weeks (The Jackson Laboratories, Bar Arbor, Maine, USA) were maintained on a 12-hr light/12-hr darkness schedule, and allowed access to food and water *ad libitum.*

Grant sponsor: Instituto de Salud Carlos III (Ciberehd); Grant number: FIS 07/0157. Grant sponsor: Consejería de Salud; Grant number: Uso Racional del Medicamento 32000/05 Centro de Investigación Biomédica en Red de Enfermedades Hepáticas y Digestivas (CIBEREHD o Ciberehd) is funded by the Instituto de Salud Carlos III.
***Correspondence to:** Unidad de Investigación, Unidad Clínica Aparato Digestivo, Hospital Universitario Reina Sofía, Av. Menéndez Pidal s/n, E-14004 Córdoba, Spain. Fax: +34-957-010452.
E-mail: jordi.muntane.exts@juntadeandalucia.es
Received 8 May 2009; Accepted after revision 20 May 2009
DOI 10.1002/ijc.24621
Published online 2 June 2009 in Wiley InterScience (www.interscience.wiley.com).

Animals were treated according to Guide of Careful and Use of Laboratory Animals of National Institute of Health (published nº 86-23, review 1985). Hepatocytes were isolated using the *in situ* collagenase perfusion procedure described by Seglen.[32] Hepatocytes (50,000 cells/cm^2) were seeded in type I collagen-coated dishes (Iwaki, Gyouda, Japan) and cultured in William's E medium (Applichem, Darmstadt, Germany) supplemented with 1 μM insulin, 0.6 μM hydrocortisone, 2 mM glutamine, 100 U/mL penicillin, 100 μg/mL streptomycin, 0.25 μg/mL amphotericin B and 5% fetal bovine serum for 2 hr in an atmosphere of 5% CO_2 at 37°C. The study was initiated 24 hr after seeding in medium without serum. Citotoxicity was induced by AFB_1 (50, 5 and 0.5 μg/mL) and the samples were collected after 12, 24 and 48 hr.

Cell line culture and treatments

Human hepatoma cell line, HepG2, was obtained of the ECACC (European Collection of Cell Cultures) and routinely maintained in MEM medium pH 7.4 supplemented with 10% fetal bovine serum, 2.2 g/L HCO_3Na, 100 mM sodium pyruvate, 0.292 gr/L glutamine, 100 U/mL penicillin, 100 μg/mL streptomycin and 0.25 μg/mL amphotericin in 5% CO_2 in air at 37°C.

Patients

Tumor and non-tumor liver sections from 22 men and 2 women who underwent orthotopic liver transplantation for HCC were collected from June 1992 to December 2003 at the Reina Sofía University Hospital. The grade of HCC differentiation was estimated according to the Edmondson-Steiner classification, and grouped as well-differentiated (Grade I–II; n = 12) or poorly differentiated (Grade III–IV; n = 12). The etiology of the patients was HBV (n = 8, 33%), HCV (n = 8, 33%) and alcohol-associated cirrhosis (n = 8, 33%). The presence of single nodule was equally distributed in well-differentiated and poorly differentiated HCC (n = 6, 50%). Nevertheless, the presence of multinodular ($\geq$3) was higher in poorly-differentiated than well differentiated HCC (n = 1, 8% *vs.* n = 3, 25%, respectively). Similarly, the presence of nodules $\geq$5 cm was higher in poorly-differentiated than well differentiated HCC (n = 0, 0% *vs.* n = 4, 33%, respectively). All patients were submitted to liver transplantation with good liver function (Child A-B) and with extensive liver cirrhosis. The patients were follow-up to 36 months. Additional demographic, clinical and pathological features of the patients are showed in Tables I and II.

Transient transfection of p27^{Kip1}

The plasmid pcDNA3 containing wild type p27^{Kip1} was provided by Dr. K.I. Nakayama (Medical Institute of Bioregulation, Kyushu, Japan).[33] The transfection was performed using Fugene 6 (Roche Molecular Biochemicals, Indianapolis, USA). HepG2 (15,000 cells/cm^2) were incubated with the transfection mixture at 37°C for 4 hr, and the study was initiated after 24 hr. The involvement of the proteasome inhibitor (PSI) on p27 degradation was assessed using Cbz-Ile-Ile-Glu(O-t-Bu)-Ala-Leucinal peptide (Calbiochem-Novabiochem Corporation, Darmstadt, Germany) (PSI, 5 μM) administered 2 hr before AFB_1.[34]

Preparation of cytoplasmic and nuclear extracts

Nuclear extracts from hepatocytes were prepared according to Schreiber *et al.*[35] Briefly, hepatocytes were recovered in 200 μL of lysis buffer (10 mM HEPES pH 7.9, 10 mM KCl, 0.1 mM EDTA, 0.1 mM EGTA, 5 μg/mL aprotinin, 10 μg/mL leupeptin, 0.5 mM phenylmethylsulfonyl fluoride, 1 mM DTT, 0.6% Nonidet NP-40) allowing to swell for 10 min on ice. After centrifugation, the supernatant (cytoplasmic fraction) was removed, and the pellet was resuspended in 25 μL of nuclear extraction buffer (20 mM HEPES pH 7.9, 0.4 mM NaCl, 1 mM EDTA, 1 mM EGTA, 5 μg/mL aprotinin, 10 μg/mL leupeptin, 0.5 mM phenylmethylsulfonyl fluoride and 1 mM DTT) for 20 min on ice and centrifuged at 15,000g for 5 min at 4°C. The supernatant (nuclear fraction) were stored at −80°C until use.

Measurement of cell death

Cellular apoptosis was determined by the measurement of hypodiploid hepatocyte population, presence of histone-associated-DNA-fragments and caspase-3 activity. Cells were recovered using cell non-enzymatic dissociation solution (Sigma Chemicals), permeabilized with 4% ethanol for 4 hr at 4°C and washed twice with PBS. HepG2 cells were sequentially incubated RNAse A (5 U/mL) and propidium iodide (20 pg/mL) for 10 min at room temperature at darkness. The fluorescence corresponding to DNA-dye complex of cell population was determined by a FACScan flow cytometer (Becton-Dickinson, San Jose, CA, USA). In this procedure, permeabilization of hepatocytes allowed leakage of small DNA fragments produced during apoptosis. Apoptotic cells appears as a subpopulation of hepatocytes with low DNA contend (hypodiploid cells). A double-discriminator module was used to distinguish between signals coming from a single cell or from those produced by cell aggregates. The histone-associated-DNA-fragments are determined using a commercial enzyme-immunoassay kit (Roche Diagnostics GmbH, Penzberg, Germany) in cell lysate, as well as the *in situ* detection in fixed cells by the terminal deoxytransferase (TdT)-mediated dUTP biotin nick end labeling (TUNEL) method (RyD Systems, Minneapolis). Caspase-3 associated activity was measured in cytoplasmic fractions (15 μg) using the corresponding peptide-based substrate (Ac-DEVD-AFC, 100 μM) (Bachem AG, Bubendorf, Switzerland). The hepatocellular necrosis was evaluated by lactate dehydrogenase (LDH) release to culture medium using a colorimetric routine laboratory method.[36]

Analysis of p21, p27, wild and mutated p53, KIST, Rsk-1 and Rsk-2 expression by western-blot

The protein expression of p21, phosphorylated (Ser 10 or S10 and Thr 198 or T198) and non phosphorylated p27, wild type and mutated p53, as well as the Ser/Thr protein kinases KIST, Rsk-1 and -2 were assessed in nuclear fraction. The protein expression of phosphorylated (T198) p27 was also assessed in cytoplasmatic fraction. Proteins (20–100 μg) were separated by 10–14% SDS-PAGE electrophoresis, transferred to nitrocellulose and submitted to Western-blot analysis using commercial polyclonal primary antibodies against p21 (sc-397, Santa Cruz Biotechnology, Santa Cruz, CA, USA), p27 (sc-528, Santa Cruz biotechnology), p27 (S10) (sc-12939-R, Santa Cruz Biotechnology), p27 (T198) (AF3994, R&D Systems, Abingdon UK), KIST (ab38292, Abcam, Cambridge, UK), Rsk-1 (sc-231, Santa Cruz Biotechnology), Rsk-2 (sc-9986, Santa Cruz Biotechnology), wild (sc-6243, Santa Cruz Biotechnology) and mutated (sc-99, Santa Cruz Biotechnology) forms of p53. The sample was incubated with the corresponding secondary antibodies labeled with horseradish peroxidase (sc-2031, Santa Cruz Biotechnology) revealing protein content by ECL. The experimental conditions of cell death and genotoxicity did not allow selecting a suitable constitutive loading control protein. In consequence, the accuracy of protein loading was followed by red pounceau.

Isolation of total RNA from formalin-fixed and paraffin-embedded tissue

Total RNA was isolated from deparaffinized formalin-fixed and dehydrated tissue (50 μm) by the High Pure FFPE RNA Micro Kit (Roche Diagnostics, Mannheim, Germany). Sections were treated with the commercial lysis buffer including SDS and proteinase K solution for 3 hr at 55°C, and the digested mixture further treated with binding buffer and ethanol, and passed through on a High Pure Filter ready to centrifuge for 30 sec at 8,000g. The retained portion in the column is treated with DNAse, and eluted with elution Buffer. RNA was stored at −80°C for later analysis.

Analysis of p21 and p27 expression by quantitative real-time RT-PCR

Total RNA in hepatocyte population was extracted using Trizol reagent according to the manufacturer's recommendations

TABLE I – CLINICAL AND PATHOLOGICAL CHARACTERISTICS OF THE PATIENTS

	Gender	Etiology	No nodules	Size (cm)	Pre-THO treatment	Post-THO treatment	Death (months)
Well-differentiated							
1	Man	HCV	1	2	IFN-α	Tacrolimus, deflazacort, sulfadoxine, pyrimethamine, methylprednisone, IFN+ribavirine	Non
2	Man	HCV	4	1.0–4	No treatment	Tacrolimus, deflazacort, sulfadoxine, pyrimethamine, methylprednisone	Non
3	Man	HCV	2	0.9–3.5	No treatment	Cyclosporine, methylprednisone	Yes (15.8)
4	Man	HCV	2	0.9–3.0	No treatment	Cyclosporine, deflazacort, sulfadoxine, pyrimethamine, IFN+ribavirine	Non
5	Man	HBV	1	3	Isoniacide	Tacrolimus, deflazacort, methylprednisone, sulfadoxine, pyrimethamine, lamivudine, γ-globulin anti-HBV	Non
6	Man	HBV	2	1.5–3.5	No treatment	Tacrolimus, methylprednisone, lamivudine, γ-globulin anti-HBV	Non
7	Man	HBV	2	0.1–3.0	No treatment	No treatment	Yes (6.2)
8	Man	HBV + HDV	2	4.5	Adriamycine + cysplatin	Cyclosporine, lamivudine, γ-globulin anti-HBV	Non
9	Man	Ethanol + HBV	1	3.5	No treatment	Tacrolimus, methylprednisone	Yes (16.0)
10	Man	Ethanol + HBV	2	1.5–2.0	No treatment	Cyclosporine, methylprednisone, deflazacort, lamivudine, γ-globulin anti-HBV, sulfadoxine, pyrimethamine	Non
11	Man	Ethanol	1	4.5	No treatment	Cyclosporine, azathioprine, methylprednisone	Non
12	Man	Ethanol	1	2.5	No treatment	Cyclosporine, azathioprine, methylprednisone	Non
Poorly-differentiated							
1	Women	HCV	2	1.5–3.0	No treatment	Cyclosporine, IFN+ribavirine	Non
2	Man	HCV	1	3	No treatment	Gancyclovir, deflazacort, cyclosporine, sulfadoxine, pyrimethamine	Non
3	Women	HCV	4 + 2	0.5 + 1.2–5.0	No treatment	Tacrolimus, mycophenolate mofetil, methylprednisone	Yes (2.9)
4	Man	HCV	1	1.8	No treatment	Tacrolimus, methylprednisone, mycophenolate mofetil	Yes (0.2)
5	Man	HBV	3	1	No treatment	Tacrolimus, methylprednisone	Yes (3.8)
6	Man	HBV	1	5.5	No treatment	Cyclosporine, methylprednisone	Non
7	Man	HBV	4	3–6.8	No treatment	No treatment	Yes (12)
8	Man	HBV	1	1	Hepatectomy 1 nodule (12 cm)	Cyclosporine, deflazacort, azathioprine, deflazacort, γ-globulin anti-HBV, Acyclovir	Non
9	Man	Ethanol	2	2.0–5.0	No treatment	Cyclosporine, methylprednisone, deflazacort, tacrolimus	Non
10	Man	Ethanol	1	3.5	No treatment	Cyclosporine	Yes (2.9)
11	Man	Ethanol	1	3	No treatment	Methylprednisone, tacrolimus	Non
12	Man	Ethanol	1	1	No treatment	Tacrolimus, mycophenolate mofetil, methylprednisone	Non

TABLE II – BIOCHEMICAL PARAMETERS OF THE PATIENTS

	Well-differentiated HCC (Grade I + II) (n = 12)	Poorly-differentiated HCC (Grade III + IV) (n = 12)
Biochemical parameters		
Age (years)	52 ± 7.3	52 ± 10.9
γ-GT (UI/L)	94 ± 41.1	118 ± 63.8
ALT (UI/L)	81 ± 53.5	103 ± 141.3
AST (UI/L)	79 ± 44.1	79 ± 79.4
Alkaline phosphatase (UI/L)	104 ± 41.1	155 ± 74.7

HCC, Hepatocellular carcinoma; HBV, Hepatitis B virus; HCV, Hepatitis C virus; γ-GT, gamma glutamyl transferase; ALT, alanine aminotransferase; AST, aspartate aminotransferase.

(Invitrogen, California, USA). RNA was treated with DNAse I (Promega, Madison, WI, USA) (1 IU/μg RNA) at 37°C for 30 min. DNAse I was degraded at 65°C for 10 min. The integrity of RNA was verified following separation by electrophoresis on 0.8% agarose gel containing 0.5 μg/mL ethidium bromide (v/v). RT-PCR was performed in one-step using the QuantiTect SYBR Green RT-PCR kit (Qiagen GmbH, Hilden, Germany) in LightCycler thermal cycler system (Roche Diagnostics). First-strand cDNA synthesis was generated from 20 ng of total RNA diluted in reaction mixture that included Omniscript and Sensiscript Reverse Transcriptase, and the specific sets of mouse p27 and p21 primers generated by the Primers 3 software supplied in the www-genome.wi.mit.edu/cgi-bin/primer/primer3_www.cgi page. The specific sets of primers for mouse p27 (sense, 5′-AGG ACG GTT TGG ATG TTT AT-3′, and antisense 5′-AGT GGG GTG ATG AGA TTT TT-3′), human p27 (sense, 5′-CTG TCC ATT TAT CCA CAG GA-3′, and antisense 5′-CCA TAC ACA GGC AAT GAA AT-3′), mouse p21 (sense 5′-ATT GCT CAG ACC TGT GAA GA-3′, and antisense 5′- AGC AGC AGA TCA CCA GAT TA-3′) and 18S (sense, 5′-GTA ACC CGT TGA ACC CCA TT-3′, and antisense, 5′-CCA TCC AAT CGG TAG TAG CG-3′) were supplied by MVG-Biotech AG (Genotek, Sabadell, Spain).

The reverse transcription was carried out at 55°C for 20 min followed by a 15 min period at 95°C. The amplification protocol consisted of 32 cycles of incubation after initial denaturation at 95°C for 15 sec (20°C/sec), 56°C for 30 sec (20°C/sec), and 72°C for 30 sec (2°C/sec). The melting conditions were fixed at 61°C (0.1°C/sec). To confirm amplification specificity, the amplified 18S product (150 bp), mouse p27 (111 bp), human p27 (123 bp) and mouse p21 (134 bp) were analyzed by 1.5% agarose gel electrophoresis containing ethidium bromide. Quantitation of relative expression was determined using the $2^{(\Delta Ct)}$ method.[37]

Thymidine incorporation assay

Hepatocytes (500,000 cells) were incubated with methyl-^{3}H-thymidine (4 μCi/mL) (Moravek Biochemical, CA, USA) for 3 hr, and lysed with 25% trichloroacetic acid and maintained at 90°C for 30 min. Sample was centrifuged at 10,000*g* for 5 min, and 25 μL of supernatant were dropped on a glass fibre filter (Wallac Oy, Turku, Finland), dried and the radioactivity detected by liquid scintillation counting in β-plate Scint (Perkin Elmer™, England).

Detection of 8-hydroxydeoxiguanosine

Hepatocytes cultured onto glass bottom culture dishes coated with collagen (MatTek Corporation, Ashland, MA, USA) were fixed, incubated with RNAse (100 μg/mL), and denatured DNA in 50 mM Tris-base. Samples were incubated with mouse monoclonal anti-8-hydroxydeoxiguanosine antibodies (R&D Systems, Abingdon UK) (1:300) at 4°C overnight, and with biotinylated anti-mouse Ig G (H+L) polyclonal antibodies (Jackson Immuno-Research Laboratories, West Grove, PA, USA) (1:500) for 30 min. Furthermore, samples were incubated with 50 μL streptavidin-horseradish peroxidase (20 μg/mL) for 30 min, and with 0.5 μg/mL diaminobenzamide tetrahydrochloride (DAB) and 0.001% hydrogen peroxide for 10 min, with further counterstaining with

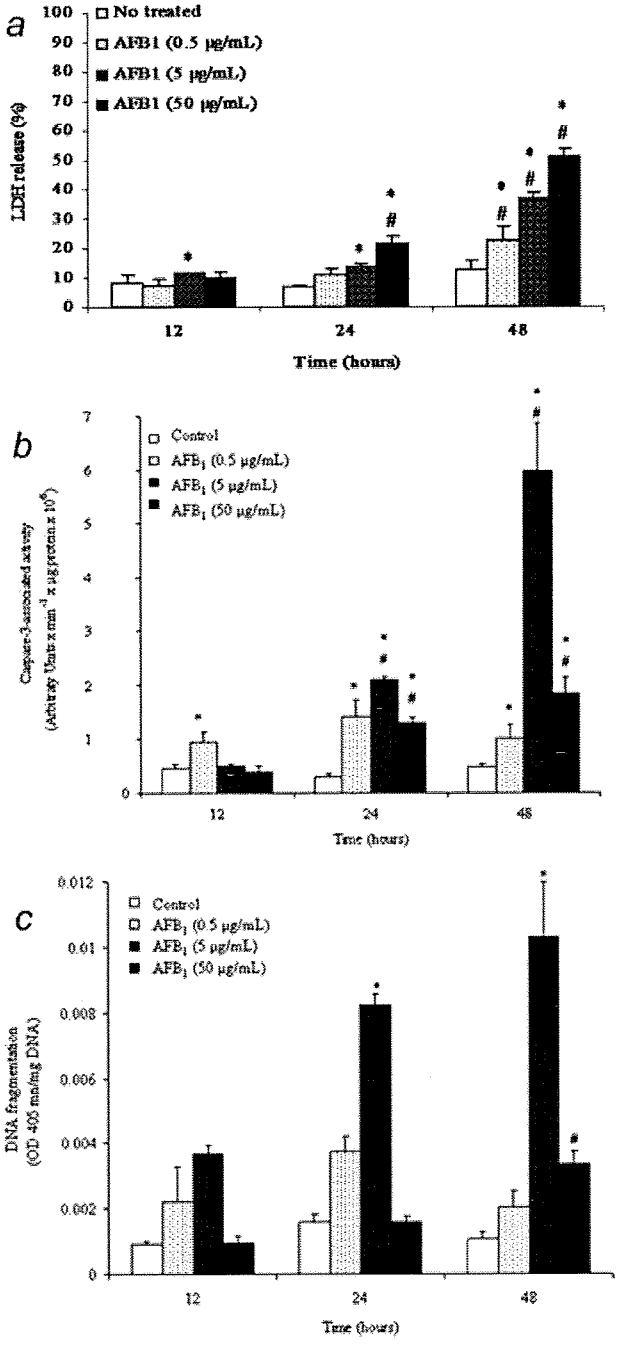

FIGURE 1 – Cell necrosis (*a*), caspase-3-associated activity (*b*) and DNA fragmentation (*c*) induced by aflatoxin B_1 (AFB_1) in primary cultured hepatocytes. AFB_1 (0, 0.5, 5 and 50 μg/mL)-treated hepatocytes were collected at different time points. Cell necrosis was evaluated by the measurement of the percentage of lactate dehydrogenase (LDH) release in cultured hepatocytes. Caspase-3 activity in cytoplasm fraction was measured by peptide-based susbtrate (Ac-DEVD-AFC). DNA fragmentation was determined with a commercial ELISA assay based on antibodies anti-histone measured by the optical density (OD) at 405 nm. Each bar represents the mean ± SE (n = 5). $^*p \leq 0.05$ *vs.* the corresponding control group. $^\#p \leq 0.05$ *vs.* the same group collected at the previous time point.

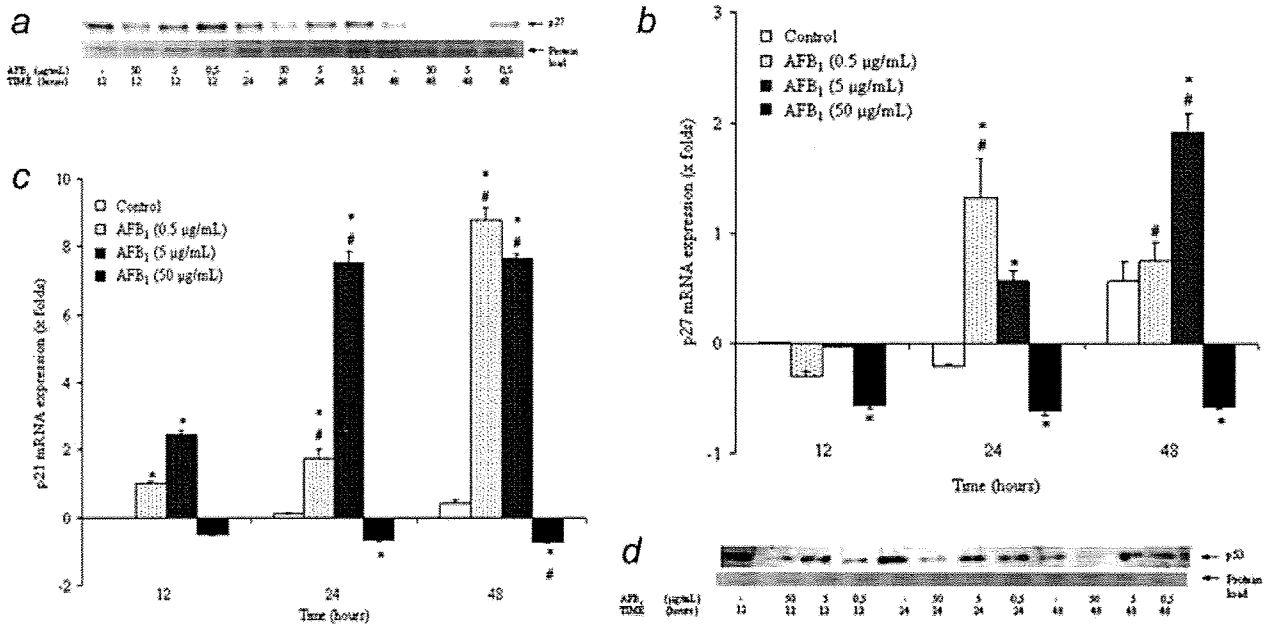

FIGURE 2 – Measurement of the p27 protein (*a*) and mRNA (*b*), p21 mRNA (*c*) and p53 protein (*d*) expression in aflatoxin B_1 (AFB_1)-treated hepatocytes. AFB_1 (0, 0.5, 5 and 50 µg/mL)-treated hepatocytes were collected at different time points. The protein expression was measured in samples (20–100 µg) by Western blot analysis using 14% SDS-PAGE electrophoresis. The mRNA expression was determined by quantitative RT-PCR, and the value is relative to that obtained in untreated samples collected at 12 hr. Bars represent the mean ± SE ($n = 5$). *$p \leq 0.05$ *vs.* control group. #$p \leq 0.05$ *vs.* the same group collected at the previous time point. The blot is representative of 5 independent experiments.

1% methyl green for 2 min. The samples were mounted with Eukkit® mounting media before observation.

Immunohistochemical detection of p21, p27 and p53 in liver sections

Deparaffinised liver sections were processed for classical immunohistochemical procedures. Samples were incubated with primary rabbit polyclonal anti-p27 (sc-528), p21 (sc-397) or p53 (sc-6243) antibodies (3 µg/mL), and with the corresponding biotinylated secondary antibodies (sc-2051). Proteins were visualized using the HRP-linked streptavidin (Santa Cruz Biothechnology) and DAB as chromogen with Gill's hematoxylin counterstaining.

Statistical analysis

Results are expressed as mean ± SE of 5 experiments. Data were compared using ANOVA with the Least Significant Difference (LSD) test as posthoc multiple comparison analysis. The statistical differences were set at $p \leq 0.05$. The groups with "a" were significantly different *vs.* the corresponding control group. The groups with "b" were significantly different *vs.* the corresponding group without AFB_1. The images or blots are representative of 5 independent experiments.

Results

Effect of AFB_1 on p27 expression and cell death in hepatocytes

AFB_1 induced a dose-dependent cell necrotic response in cultured hepatocytes (Fig. 1*a*) ($p \leq 0.05$). AFB_1 also enhanced caspase-3 activity (Fig. 1*b*) and the presence of histone-associated DNA fragments (Fig. 1*c*) in cell lysate. The highest apoptotic cell signal was observed in the intermediate AFB_1 (5 µg/mL) concentration (Figs. 1*b* and 1*c*) related to a reduction of p27 protein (Fig. 2*a*) expression and a rise of p27 mRNA (Fig. 2*b*) expression in hepatocytes. The highest necrotic response was observed at the highest AFB_1 (50 µg/mL) concentration (Fig. 1*a*) that was related to a drastic reduction of cellular apoptosis (Figs. 1*b* and 1*c*) and p27 protein (Fig. 2*a*) and mRNA (Fig. 2*b*) expression in cultured hepatocytes. The data suggest that the exacerbation of cell death by AFB_1 was accompanied of an intense degradation of p27 expression. The induction of cell death by AFB_1 induced a similar profile on p21 (Fig. 2*c*) and p53 (Fig. 2*d*) expression than that observed for p27 expression. Nevertheless, p21 protein expression was not detected in cultured hepatocytes (data not shown).

Role of p27 deficiency on AFB_1-induced cell death in hepatocytes

The role of p27 on AFB_1-induced genotoxicity was addressed in cultured hepatocytes isolated from p27-deficient mice. The study showed that p27 deficiency enhanced AFB_1-induced cell death. In this sense, p27 deficiency enhanced the levels of LDH release (Fig. 3*a*) and caspase-3 activity (Fig. 3*b*) in AFB_1 (5 µg/mL)-induced cell death in hepatocytes. This noxious effect of p27 deficiency was related to an increase of cell proliferation (Fig. 4*a*) and the accumulation of DNA damage (Fig. 4*b*) in AFB_1-treated hepatocytes. The deficiency of p27 enhanced the percentage of 8-hydroxydeoxiguanosine positive cells compared to control AFB_1 (5 µg/mL)-treated hepatocytes (47 ± 1.4 *vs.* 28 ± 1%). Interestingly, the reduction of cell proliferation (Fig. 4*a*) by p27 deficiency was related to an increase of p21 expression (Fig. 5). The expression of p27 (protein and mRNA) was not detected in p27 deficient hepatocytes (data not shown). The intermediate concentration of AFB_1 (5 µg/mL) reduced p21 protein (Fig. 5*a*) and enhanced p21 mRNA (Fig. 5*b*) expression in p27 deficient hepatocytes. The pro-necrotic toxin concentration (50 µg/mL) reduced both p21 protein and mRNA expression in p27 deficient hepatocytes (Figs. 5*a* and 5*b*). The regulation of p53 expression by AFB_1 followed the same profile as described for p21 in p27 deficient hepatocytes (Fig. 5*c*).

Role of p27 overexpression on AFB_1-induced cell death in HepG2 cells

The transfection with wild type $p27^{Kip1}$ expression vector enhanced p27 protein expression in HepG2 (Fig. 6*a*). The absence

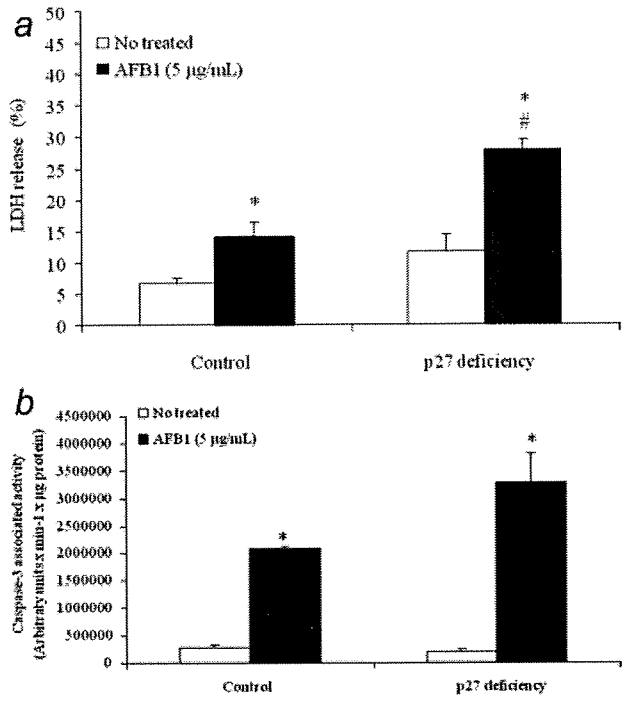

FIGURE 3 – Cell necrosis (*a*) and caspase-3-associated activity (*b*) induced by aflatoxin B_1 (AFB_1) in primary control and p27-deficient cultured hepatocytes. AFB_1 (0 and 5 µg/mL)-treated hepatocytes were collected at 24 hr. Cell necrosis was evaluated by the measurement of the percentage of lactate dehydrogenase (LDH) release in cultured hepatocytes. Caspase-3 activity in cytoplasm fraction was measured by peptide-based susbtrate (Ac-DEVD-AFC). Data are mean ± SE (n = 4). *$p \leq 0.05$ doses AFB_1 *vs.* control group. #$p \leq 0.05$ p27 deficiency *vs.* control group.

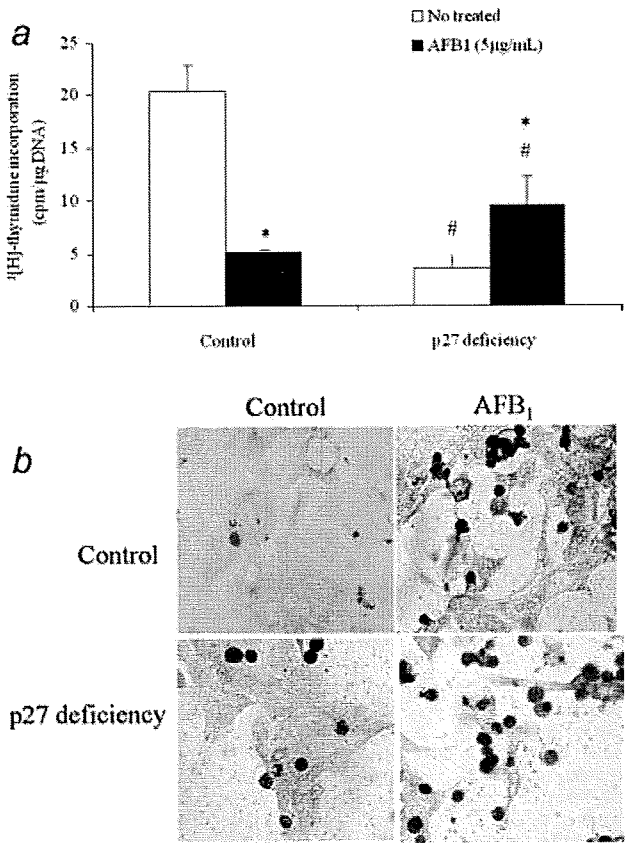

FIGURE 4 – Cell proliferation (*a*) and DNA damage (*b*) induced by aflatoxin B_1 (AFB_1) in primary control and p27-deficient cultured hepatocytes. AFB_1 (0 and 5 µg/mL)-treated hepatocytes are collected at 24 hr. Cell proliferation was assessed by the measurement of ^{3}[H]-thymidine incorporation. DNA damage was identified as the presence of 8-hydroxydeoxiguanosine positive cells. Data are the mean ± SE (n = 5). *$p \leq 0.05$ *vs.* untreated cells. #$p \leq 0.05$ p27 deficiency *vs.* control group. The images are representative of 3 independent experiments (original magnification, ×20). [Color figure can be viewed in the online issue, which is available at www.interscience.wiley.com.]

of p27 expression was associated with p21 (Fig. 6*b*) and p53 (Fig. 6*c*) expression in HepG2 cells. AFB_1 (5 µg/mL) enhanced p21 (Fig. 6*b*) and p53 (Fig. 6*c*) expression in HepG2. The highest AFB_1 (5 µg/mL) concentration enhanced p27 (Fig. 6*a*) and p21 (Fig. 6*b*) degradation in $p27^{kip1}$-transfected HepG2 cells. Differently, the expression of p53 was enhanced by the highest AFB_1 concentration, although the values were below that those obtained in the intermediate AFB_1 concentration (Fig. 6*c*). The prevention of p27 degradation by PSI only increased the expression of p27 in $p27^{kip1}$-tranfected cells, but not in control cells suggesting that p27 was not expressed in resting cells (Fig. 6*d*). The overexpression of p27 reduced the percentage of hypodiploid cells at 12 and 24 hr after AFB_1 (5 µg/mL) toxicity (Fig. 7*a*). The overexpression of p27 also reduced caspase-3 activity (Fig. 7*b*), TUNEL staining (Fig. 7*c*) and DNA mutagenesis (Fig. 7*d*) in AFB_1 (5 and 50 µg/mL) -treated HepG2. The p27 overexpression reduced the percentage of TUNEL and 8-hydroxydeoxiguanosine positive cells compared to control AFB_1 (50 µg/mL)-treated hepatocytes (1 ± 0.6 *vs.* 80 ± 5.6% and 28 ± 13.0 *vs.* 76 ± 7.3%, respectively). This beneficial effect of p27 was related to a reduction on cell proliferation (Fig. 7*e*) in AFB_1-treated HepG2 cells.

Expression of KIST and RSK-1 and -2, and post-translational phosphorylation of p27

The expression of KIST, RSK-1 and -2, and p27 phosphorylation (S10 and T198) was determined shortly after AFB_1 toxicity in HepG2 cells. The p27 balance is fine-tuned by multiple post-translational modifications that affect the function of p27 by altering protein-protein interactions, affecting subcellular localization and modulating protein stability. The expression level is due to enhanced p27 mRNA translation and stabilization of the protein as a result of phosphorylation at S10 and T198. The first S10 kinase identified was kinase interacting stathmin (KIST), a nuclear enzyme that is activated in response by mitogens during G0–G1 transition.[38] The nuclear expression of KIST (Fig. 8*a*) was related to enhanced S10 phosphorylation of p27 (Fig. 8*b*) in control p27-overexpressed HepG2 cells. Nevertheless, the rapid stimulation of KIST expression (Fig. 8*a*) by AFB_1 (5 µg/mL) was related to a clear reduction of S10 phosphorylation of p27 (Fig. 8*b*) in nuclear fraction. This effect paralleled the reduction of total p27 expression in nuclear fraction induced by AFB_1 from p27-overexpressed HepG2 cells (Fig. 8*c*). In addition to S10, T198, which is phosphorylated in G0 is also subject to modification early in G1. At least 3 kinases have been demonstrated to phosphorylated p27 at T198, including AKT, Rsk-1 and Rsk-2.[39,40] The expression of T198 p27 phosphorylated form was never detected in nuclear fraction (data not shown). Differently, a mild progressive accumulation of T198 p27 phosphorylated form was detected in cytoplasmatic fraction from control p27-overexpressed cells (Fig. 8*d*). Interestingly, a rapid accumulation of T198 p27 phosphorylated form in cytoplasm was already detected 1 hr after the addition of AFB_1 in HepG2 cells (Fig. 8*d*) that was associated to enhanced Rsk-1 and -2 expression in nuclear fraction (Fig. 8*e*).

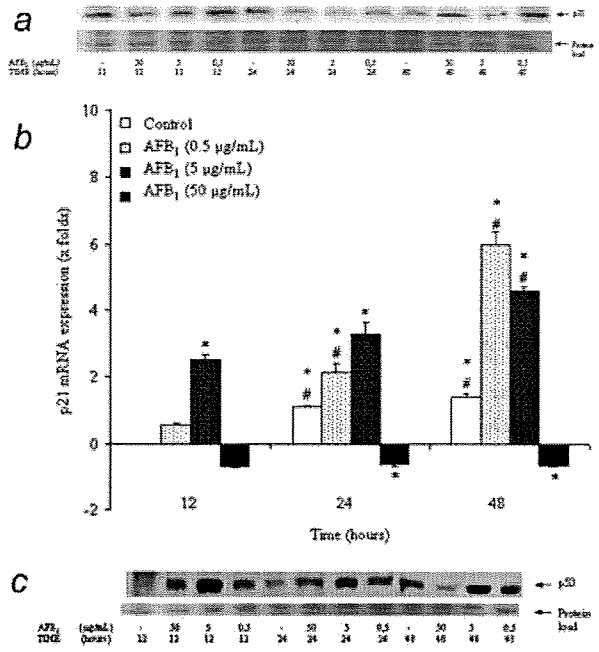

FIGURE 5 – Measurement of the p21 protein (*a*) and mRNA (*b*), and p53 protein (*c*) expression in aflatoxin B1 (AFB_1)-treated p27 deficient hepatocytes. AFB_1 (0, 0.5, 5 and 50 μg/mL)-treated hepatocytes were collected at different time points. The protein expression was measured in samples (20–100 μg) by Western blot analysis using 14% SDS-PAGE electrophoresis. The mRNA expression was determined by quantitative RT-PCR, and the value is relative to that obtained in untreated samples collected at 12 hr. The blot is representative of 5 independent experiments. Data are the mean ± SE ($n = 5$). *$p \leq 0.05$ *vs.* control group. #$p \leq 0.05$ *vs.* the same group collected at the previous time point.

p27, p21 and p53 expression was related to the stage of tumor differentiation and patient survival

The main clinical and biochemical data of the patients are shown in Tables I and II. The patients with poorly differentiated tumors showed a reduced survival than patients with well differentiated tumors (Fig. 9*a*). The lower survival of patients with poorly-differentiated stage of HCC was related to low expression of p27, p21 and p53 in peritumoral and tumoral area of HCC (Fig. 9*b*). The images correspond to the patient 2 (well differentiated) and 3 (poorly-differentiated) that have a similar number and sizes of nodules. The tumoral tissue mRNA p27 expression in well differentiated patient is 6.53-folds (13.0 ± 1.30 *vs.* 2.01 ± 0.05 ΔCt) compared to that observed in poorly-differentiated tumors.

Discussion

HCC is the sixth most commonly occurring cancer in the world and the third greatest cause of cancer mortality.[1,2] The regulation of cell cycle is a key factor for the maintenance of cell growth and protects the cell from DNA damage. Beside different biochemical markers, several cell cycle regulators such as p27 and p53 have been identified as potential prognostic markers for the outcome of HCC.[9,28,41] The pathogenesis of HCC is related to environmental, infectious, nutritional, metabolic and endocrine factors that contribute directly or indirectly to hepatocarcinogenesis. The adverse health effects associated with AFB_1 exposures range from acute liver toxicities to liver cancer. The induction of advanced genotoxicity by AFB_1 was related to DNA damage accumulation, hepatocellular necrosis and reduction of p27 expression in hepatocytes. AFB_1-induced nuclear phosphorylated (S10) p27 degradation was related to a rise of nuclear KIST, Rsk-1 and Rsk-2 expression and cytoplasm phosphorylated (T198) p27 expression. The overexpression of p27 reduced cellular proliferation, apoptosis and DNA mutagenesis induced by AFB_1 in hepatocytes. The analysis of human HCC tissue showed that the expression of p27, p21

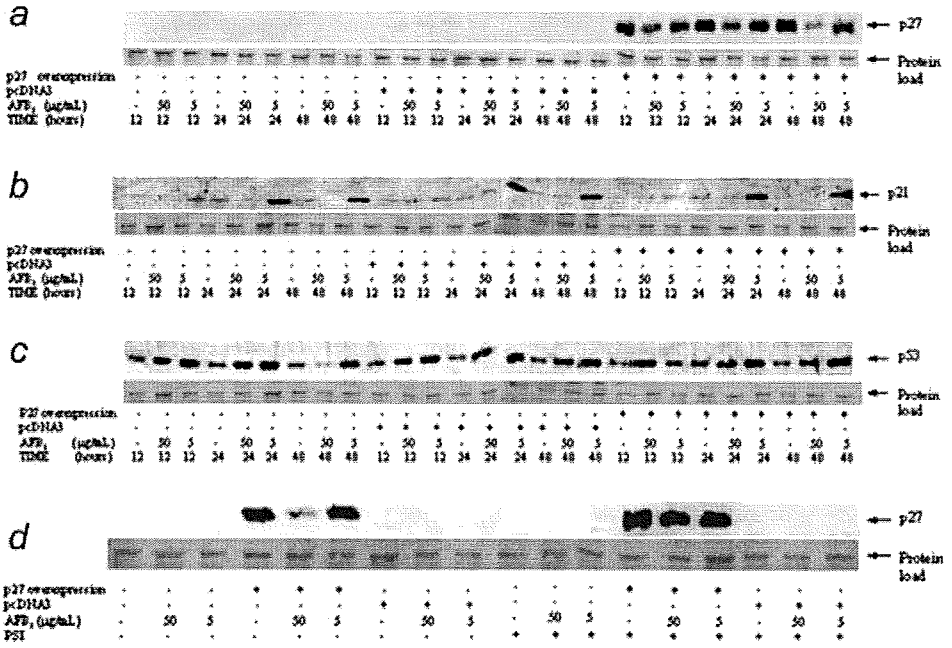

FIGURE 6 – Measurement of p27 (*a*), p21 (*b*) and p53 protein (*c*) expression in aflatoxin B_1 (AFB_1)-treated control and transiently p27-expressing vector transfected HepG2 cells. AFB_1 (0, 5 and 50 μg/mL)-treated hepatocytes were collected at different time points. Effect of proteasome inhibitor (PSI) in the p27 protein expression in control and transiently p27-expressing vector transfected HepG2 cells (*d*). AFB_1 (0, 5 and 50 μg/mL)-treated hepatocytes were collected at 48 hr. The expression of p27, p21 and p53 was measured in nuclear fraction by SDS-PAGE electrophoresis coupled to Western blot analysis. The image is representative of 5 independent experiments.

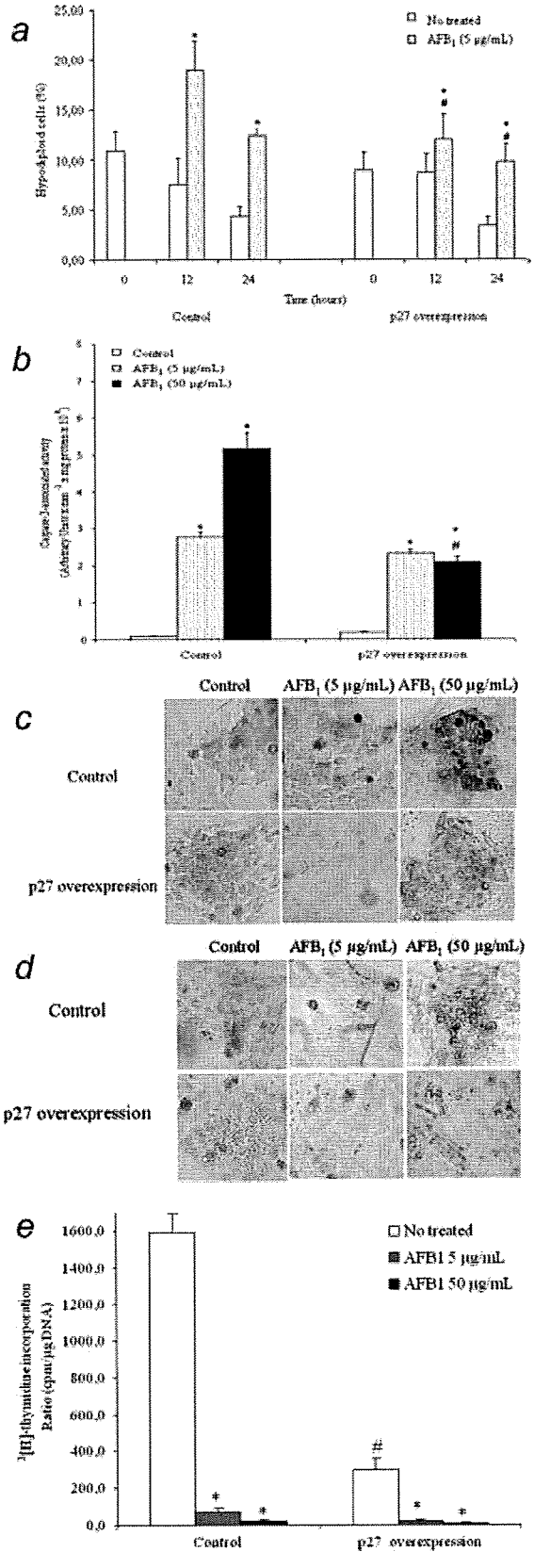

and p53 was related to well differentiated stages and extended survival of the patients.

The human exposure to foodstuffs contaminated with mycotoxin AFB_1 is a risk factor for the development of HCC, in part because *in vitro* experiments have demonstrated that AFB_1 mutagenic metabolites bind to DNA and are capable of inducing G-to-T transversions.[42] We could not detect mutated p53 protein expression, characteristic of AFB_1 genotoxicity, but the expression of wild p53 expression paralleled that of p21 or p27 expression. The expression of p21, but not p27, has been related to hepatocellular proliferation in experimental liver resection.[43,44] Nevertheless, p27 mRNA and protein expression is enhanced in EGF-stimulated hepatocytes.[45] Genotoxic stress induced by DNA damaging chemicals causes a variety of cellular and molecular responses in mammalian cells, including cell cycle arrest, DNA repair and apoptosis.[46] The induction of low hepatocellular damage is related to enhanced p27 mRNA and protein expression in AFB_1-treated hepatocytes. Nevertheless, the extensive hepatocellular necrosis and DNA damage accumulation by the high AFB_1 concentration was related to a reduction of p27 expression and cell proliferation. The effect of AFB_1 on p21 mRNA expression was similar to that observed in p27 in hepatocytes. Nevertheless, p21 protein expression was absent in cultured mouse hepatocytes suggesting that p21 expression was negatively post-transcriptionally regulated in p27-expressing cells. The elevation of p27 and p21 by proteasome inhibition induced cell cycle arrest and apoptosis in human Jurkat T cells.[47] Our data showed that the reduction of p27 expression during AFB_1-induced genotoxicity is associated with cell cycle arrest in hepatocytes. The treatment with PSI was not able to rescue the levels of p27 in HepG2 cells suggesting that its expression/function may be replaced by p21 in this cell line. In this sense, p21 expression functions to maintain quiescence of

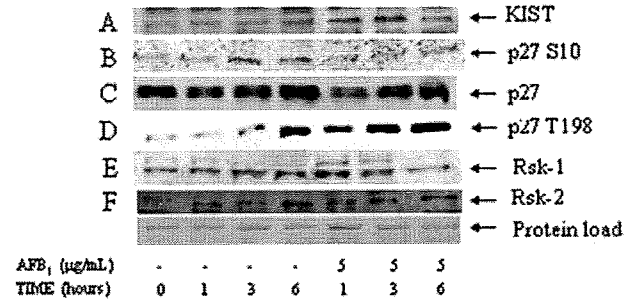

FIGURE 8 – Measurement of KIST (*a*), phosphorylated p27 (Serine 10 or S10) (*b*), p27 (*c*), phosphorylated p27 (Threonine 198 or T198) (*d*), Rsk-1 (*e*) and Rsk-2 (*f*) expression in aflatoxin B_1 (AFB_1)-treated HepG2 cells. AFB_1 (0 and 5 µg/mL)-treated hepatocytes were collected at different time points. The expression of KIST, p27 (S10), p27, Rsk-1 and Rsk-2 was measured in nuclear fraction and p27 (T198) in cytoplasm by SDS-PAGE electrophoresis coupled to Western blot analysis. The image is representative of 5 independent experiments.

FIGURE 7 – Measurement of hypodiploid cells (*a*), caspase-3-associated activity (*b*), apoptotic cells (*c*), DNA damage (*d*) and cell proliferation (*e*) in aflatoxin B_1 (AFB_1)-treated HepG2 cells transiently transfected with p27 expressing vector. Samples from AFB_1 (5 and 50 µg/mL)-treated hepatocytes were collected at 24 hr. Caspase-3 activity in cytoplasm fraction was measured by peptide-based substrate (Ac-DEVD-AFC). Hypodiploid cells and apoptotic cells were determined by flow cytometry and TUNEL staining, respectively. DNA damage was identified as the presence of 8-hydroxydeoxiguanosine positive cells. DNA synthesis was evaluated as the incorporation of ^{3}[H]-thymidine to HepG2 cells. Each bar represents the mean ± SE (n = 4). $^*p \leq 0.05$ doses AFB_1 *vs.* no treated. $^\#p \leq 0.05$ p27 deficiency *vs.* its corresponding control group. The images are representative of 3 independent experiments (original magnification, ×20). [Color figure can be viewed in the online issue, which is available at www.interscience.wiley.com.]

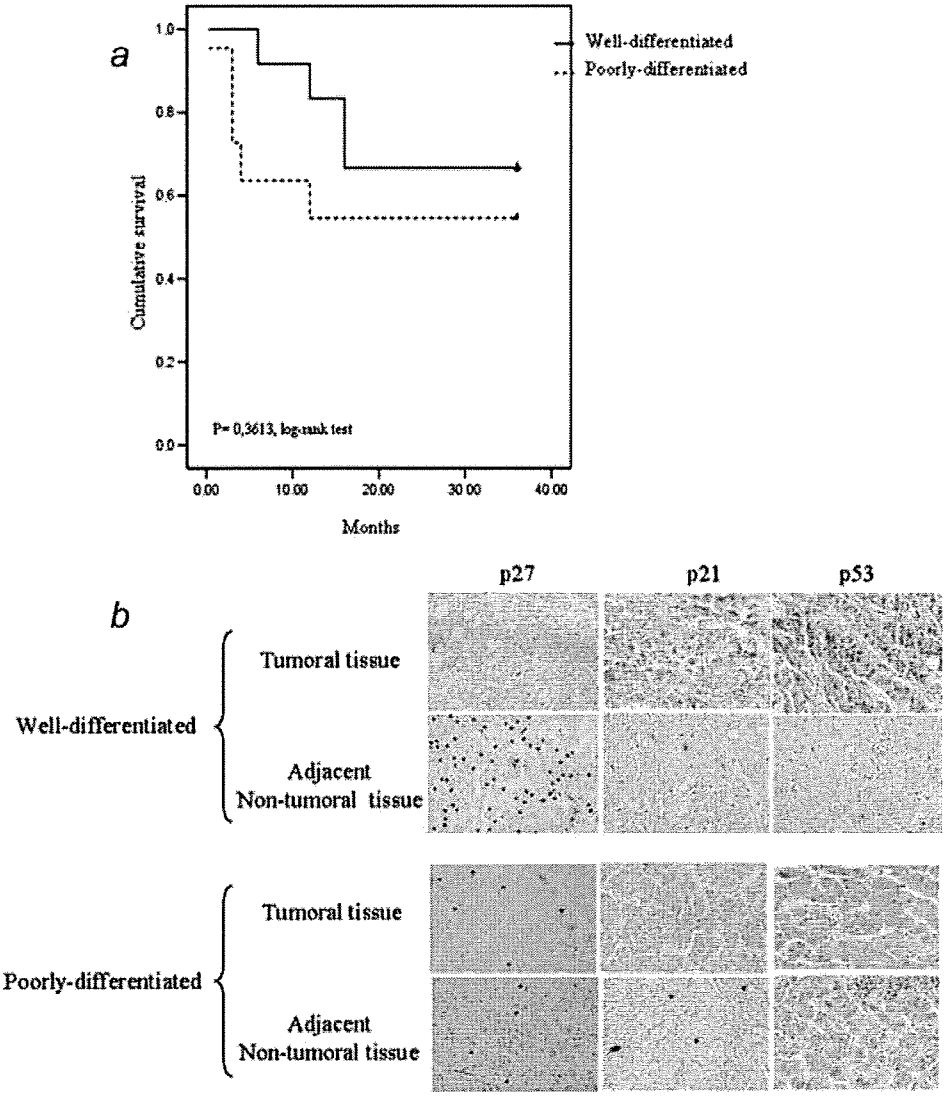

FIGURE 9 – Kaplan-Meier survival curves of well- and poorly-differentiated hepatocarcinoma (HCC) (*a*). The statistical analysis was carried out by log-rank test with 0.83 as value for the statistic ($p \leq 0.3613$). p27, p21 and p53 protein expression in well- and poorly-differentiated HCC with the corresponding adjacent non-tumoral tissue (*b*). Samples were obtained from patients with well- ($n = 8$) and poorly-differentiated ($n = 8$) HCC from different etiologies. The expression was analyzed by immunohistochemistry with 3, 3'-diaminobenzidine staining in liver sections. The images are representative of 4 different assays (original magnification, ×40). [Color figure can be viewed in the online issue, which is available at www.interscience.wiley.com.]

p27-deficient hepatocytes.[48] It has been proposed that the expression of p21 is regulated by p53, transforming growth factor-β (TGF-β), differentiation and cellular senescence.[49] But, the expression of p21 and p53 were not correlated in primary culture of mouse hepatocytes. Differently, the intermediate AFB_1 concentration dramatically increases p53 and p21 expression in HepG2 cells. In this sense, our study suggests that p53 regulates the expression of p21 in hepatocarcinoma cell line, but not in primary culture mouse hepatocytes. The deficiency of p27 enhanced cell proliferation in AFB_1-treated hepatocytes. This effect may be related to the concomitant reduction of p21 expression in injured hepatocytes. Kwon *et al.*[48] showed that cell proliferation only increases in both p21 and p27 deficient mice. The overexpression of p27 reduced cell proliferation in control and AFB_1-treated hepatocytes. Although, p21 and p27 activities are mostly concerned to their role on cell cycle control, they have also been implicated in the induction of apoptosis. In this sense, p21 has been related to inhibition of apoptosis in a number of systems, and this may counteract its tumor suppressive function as a growth inhibitor.[50] Kwon *et al.*[51] have related the anti-apoptotic effect of p21 to its absolute requirement for the induction of hepatocellular necrosis during CCl_4-induced liver injury. Nevertheless, hepatocellular necrosis is observed in the absence of p21 protein expression in AFB_1-treated hepatocytes. The expression of p27 is maintained in quiescent liver, but it decreases prior to the rise of necrotic marker in CCl_4-treated mice.[51] The primary signal for AFB_1-induced apoptosis was related to enhanced p27 expression, but necrosis was associated with a reduced expression of p27 in hepatocytes. The highest pro-apoptotic signal was related to an increase of p53 and p21 in HepG2 cells.

The induction of genotoxicity by AFB_1 was related to DNA damage accumulation, hepatocellular necrosis and reduction of p27 expression in hepatocytes. The p27 balance is fine-tuned by multiple post-translational modifications that affect the function of

p27 by altering protein-protein interactions, affecting subcellular localization and modulating protein stability. The expression of KIST, Rsk-1 and -2, and p27 phosphorylation (S10 and T198) was determined shortly after AFB_1 toxicity in HepG2 cells. The degradation of nuclear phosphorylated (S10) p27 was related to a rise of nuclear KIST, Rsk-1 and Rsk-2 expression and cytoplasm phosphorylated (T198) p27 expression in AFB_1-treated HepG2 cells. The deficiency of p27 enhanced DNA damage in control and AFB_1-treated hepatocytes. By contrast, the overexpression of p27 reduced DNA damage in AFB_1-treated HepG2 cells. Payne *et al.*[52] have recently observed that p27 deficient mice also displayed a higher *N*-ethyl-*N*-nitrosourea-induced mutation frequency in the colon. The analysis of tumoral and non-tumoral area of biopsies obtained from patients submitted to liver resection for HCC showed that the poorly differentiated tumors presented low degree of p27, p21 and p53 expression. The underexpression of p27 has been related to more severe tumor grade and as a negative prognostic marker in HCC.[25–28]

The present study supports the important role of p27 in the prevention of the experimental genotoxicity. Thus, p27 exerts a beneficial activity by 2 mechanisms. The first is by reducing the proliferation of cells that have already sustained an oncogenic lesion. The second is by transient inhibition of cell cycle progression following genotoxic insult, thereby minimizing DNA damage and fixation of mutations. Both effects led to an additional reduction of cell death during AFB_1-induced genotoxicity.

References

1. Anthony PP. Hepatocellular carcinoma: an overview. Histopathology 2001;39:109–18.
2. Parkin DM, Bray F, Ferlay J, Pisani P. Global cancer statistics, 2002. CA Cancer J Clin 2005;55:74–108.
3. Llovet JM, Bruix J. Novel advancements in the management of hepatocellular carcinoma in 2008. J Hepatol 2008;48:S20–S37.
4. Mise K, Tashiro S, Yogita S, Wada D, Harada M, Fukuda Y, Miyake H, Isikawa M, Izumi K, Sano N. Assessment of the biological malignancy of hepatocellular carcinoma: relationship to clinicopathological factors and prognosis. Clin Cancer Res 1998;4:1475–82.
5. Bismuth H, Majno PE, Adam R. Liver transplantation for hepatocellular carcinoma. Semin Liver Dis 1999;19:311–22.
6. Llovet JM, Bruix J, Gores GJ. Surgical resection versus transplantation for early hepatocellular carcinoma: clues for the best strategy. Hepatology 2000;31:1019–21.
7. Imamura H, Matsuyama Y, Tanaka E, Ohkubo T, Hasegawa K, Miyagawa S, Sugawara Y, Minagawa M, Takayama T, Kawasaki S, Makuuchi M. Risk factors contributing to early and late phase intrahepatic recurrence of hepatocellular carcinoma after hepatectomy. J Hepatol 2003;38:200–7.
8. Llovet JM, Bruix J. Systematic review of randomized trials for unresectable hepatocellular carcinoma: chemoembolization improves survival. Hepatology 2003;37:429–42.
9. Tanaka S, Toh Y, Adachi E, Matsumata T, Mori R, Sugimachi K. Tumor progression in hepatocellular carcinoma may be mediated by p53 mutation. Cancer Res 1993;53:2884–7.
10. Piao Z, Kim H, Jeon BK, Lee WJ, Park C. Relationship between loss of heterozygosity of tumor suppressor genes and histologic differentiation in hepatocellular carcinoma. Cancer 1997;80:865–72.
11. Gorrin Rivas MJ, Arii S, Furutani M, Harada T, Mizumoto M, Nishiyama H, Fujita J, Imamura M. Expression of human macrophage metalloelastase gene in hepatocellular carcinoma: correlation with angiostatin generation and its clinical significance. Hepatology 1998;28:986–93.
12. Ito Y, Matsuura N, Sakon M, Miyoshi E, Noda K, Takeda T, Umeshita K, Nagano H, Nakamori S, Dono K, Tsujimoto M, Nakahara M, et al. Expression and prognostic roles of the G1-S modulators in hepatocellular carcinoma: p27 independently predicts the recurrence. Hepatology 1999;30:90–9.
13. Tannapfel A, Wasner M, Krause K, Geissler F, Katalinic A, Hauss J, Mössner J, Engeland K, Wittekind C. Expression of p73 and its relation to histopathology and prognosis in hepatocellular carcinoma. J Natl Cancer Inst 1999;91:1154–8.
14. Suda T, Isokawa O, Aoyagi Y, Nomoto M, Tsukada K, Shimizu T, Suzuki Y, Naito A, Igarashi H, Yanagi M, Takahashi T, Asakura H. Quantitation of telomerase activity in hepatocellular carcinoma: a possible aid for a prediction of recurrent diseases in the remnant liver. Hepatology 1998;27:402–6.
15. Jackson PE, Groopman JD. Aflatoxin and liver cancer. Baillieres Best Pract Res Clin Gastroenterol 1999;13:545–55.
16. Garner RC, Miller EC, Miller JA. Liver microsomal metabolism of aflatoxin B1 to a reactive derivative toxic to *Salmonella typhimurium* TA 1530. Cancer Res 1972;32:2058–66.
17. Hsu IC, Metcalf RA, Sun T, Welsh JA, Wang NJ, Harris CC. Mutational hotspot in the p53 gene in human hepatocellular carcinomas. Nature 1991;350:427–8.
18. Bressac B, Kew M, Wands J, Ozturk M. Selective G to T mutations of p53 gene in hepatocellular carcinoma from southern Africa. Nature 1991;350:429–31.
19. Tashiro F, Morimura S, Hayashi K, Makino R, Kawamura H, Horikoshi N, Nemoto K, Ohtsubo K, Sugimura T, Ueno Y. Expression of the c-Ha-ras and c-myc genes in aflatoxin B1-induced hepatocellular carcinomas. Biochem Biophys Res Commun 1986;138:858–64.
20. Grana X, Reddy EP. Cell cycle control in mammalian cells: role of cyclins, cyclin dependent kinases (CDKs), growth suppressor genes and cyclin-dependent kinase inhibitors (CKIs). Oncogene 1995;11:211–19.
21. Obaya AJ, Sedivy JM. Regulation of cyclin-Cdk activity in mammalian cells. Cell Mol Life Sci 2002;59:126–42.
22. Sherr CJ, Roberts JM. CDK inhibitors: positive and negative regulators of G1-phase progression. Genes Dev 1999;13:1501–12.
23. Soos TJ, Kiyokawa H, Yan JS, Rubin MS, Giordano A, DeBlasio A, Bottega S, Wong B, Mendelsohn J, Koff A. Formation of p27-CDK complexes during the human mitotic cell cycle. Cell Growth Differ 1996;7:135–46.
24. Toyoshima H, Hunter T. p27, a novel inhibitor of G1 cyclin-Cdk protein kinase activity, is related to p21. Cell 1994;78:67–74.
25. Cheng M, Sexl V, Sherr CJ, Roussel MF. Assembly of cyclin D-dependent kinase and titration of p27Kip1 regulated by mitogen-activated protein kinase kinase (MEK1). Proc Natl Acad Sci USA 1998;95:1091–6.
26. Slingerland J, Pagano M. Regulation of the cdk inhibitor p27 and its deregulation in cancer. J Cell Physiol 2000;183:10–17.
27. Qin LF, Ng IO. Expression of p27 (KIP1) and p21 (WAF1/CIP1) in primary hepatocellular carcinoma: clinicopathologic correlation and survival analysis. Hum Pathol 2001;32:778–84.
28. Tannapfel A, Grund D, Katalinic A, Uhlmann D, Kockerling F, Haugwitz U, Wasner M, Hauss J, Engeland K, Wittekind C. Decreased expression of p27 protein is associated with advanced tumor stage in hepatocellular carcinoma. Int J Cancer 2000;89:350–5.
29. Fiorentino M, Altimari A, D'Errico A, Cukor B, Barozzi C, Loda M, Grigioni WF. Acquired expression of p27 is a favorable prognostic indicator in patients with hepatocellular carcinoma. Clin Cancer Res 2000;6:3966–72.
30. Armengol C, Boix L, Bachs O, Sole M, Fuster J, Sala M, Llovet JM, Rodés J, Bruix J. p27(Kip1) is an independent predictor of recurrence after surgical resection in patients with small hepatocellular carcinoma. J Hepatol 2003;38:591–7.
31. Vervoorts J, Lüscher B. Post-translational regulation of the tumor supperssor $p27^{KIP1}$. Cell Mol Life Sci 2008;65:3255–64.
32. Seglen PO. Preparation of isolated rat liver cells. Methods Cell Biol 1976;13:29–83.
33. Guan XX, Chen LB, Ding GX, De W, Zhang AH. Transfection of p27kip1 enhances radiosensitivity induced by ^{60}Co gamma-irradiation in hepatocellular carcinoma HepG2 cell line. World J Gastroenterol 2004;10:3103–6.
34. Pagano M, Tam SW, Theodoras AM, Beer-Romero P, Del SG, Chau V, Yew PR, Draetta GF, Rolfe M. Role of the ubiquitin-proteasome pathway in regulating abundance of the cyclin-dependent kinase inhibitor p27. Science 1995;269:682–5.
35. Schreiber E, Matthias P, Muller MM, Schaffner W. Rapid detection of octamer binding proteins with 'mini-extracts', prepared from a small number of cells. Nucleic Acids Res 1989;17:6419.
36. Taffs RE, Sitkovsky M. In vitro assays for mouse B and T lymphocyte function. New York: Greene Publishing, 1991.3.16.1–3.16.8.
37. Pedersen SB, Amtssygehus A. Multiplex relative gene expression analysis by real-time RT-PCR using the iCycler iQ detection system, 107th edn. New York: Cold Spring Harbor Press and Higwire Press, 2001.10–14.
38. Boehm M, Yoshimoto T, Crook MF, Nallamshetty S, True A, Nabel GJ, Nabel EG. A growth factor-dependent nuclear kinase phosphorylates p27 (kip1) and regulates cell cycle progression. EMBO J 2002;21:3390–401.
39. Fujita N, Sata S, Katayama K, Tsuruo T. Akt-dependent phosphorylation of p27Kip1 promotes binding to 14-3-3 and cytoplasmic localization. J Biol Chem 2002;277:28706–13.

40. Fujita N, Sata S, Katayama K, Tsuruo T. Phosphorylation of p27kip1 at threonine 198 by p90 ribosomal protein S6 kinase promotes its binding to 14-3-3 and cytoplasmic localization. J Biol Chem 2003; 278:49254–60.
41. Ito Y, Matsuura N, Sakon M, Miyoshi E, Noda K, Takeda T, Umeshita K, Nagano H, Nakamori S, Dono K, Tsujimoto M, Nakahara M, et al. Expression and prognostic roles of the G1-S modulators in hepatocellular carcinoma: p27 independently predicts the recurrence. Hepatology 1999;30:90–9.
42. Foster PL, Eisenstadt E, Miller JH. Base substitution mutations induced by metabolically activated aflatoxin B1. Proc Natl Acad Sci USA 1983;80:2695–8.
43. Albrecht JH, Poon RY, Ahonen CL, Rieland BM, Deng C, Crary GS. Involvement of p21 and p27 in the regulation of CDK activity and cell cycle progression in the regenerating liver. Oncogene 1998;16: 2141–50.
44. Kato A, Ota S, Bamba H, Wong RM, Ohmura E, Imai Y, Matsuzaki F. Regulation of cyclin D-dependent kinase activity in rat liver regeneration. Biochem Biophys Res Commun 1998;245: 70–4.
45. Ilyin GP, Glaise D, Gilot D, Baffet G, Guguen-Guillouzo C. Regulation and role of p21 and p27 cyclin-dependent kinase inhibitors during hepatocyte differentiation and growth. Am J Physiol Gastrointest Liver Physiol 2003;285:G115–27.
46. Islaih M, Halstead BW, Kadura IA, Li B, Reid-Hubbard JL, Flick L, Altizer JL, Thom Deahl J, Monteith DK, Newton RK, Watson DE. Relationships between genomic, cell cycle, and mutagenic responses of TK6 cells exposed to DNA damaging chemicals. Mutat Res 2005; 578:100–16.
47. Chen WJ, Lin JK. Induction of G1 arrest and apoptosis in human jurkat T cells by pentagalloylglucose through inhibiting proteasome activity and elevating p27Kip1, p21Cip1/WAF1, and Bax proteins. J Biol Chem 2004;279:13496–505.
48. Kwon YH, Jovanovic A, Serfas MS, Kiyokawa H, Tyner AL. p21 functions to maintain quiescence of p27-deficient hepatocytes. J Biol Chem 2002;277:41417–22.
49. Lee MH, Reynisdottir I, Massague J. Cloning of p57KIP2, a cyclin-dependent kinase inhibitor with unique domain structure and tissue distribution. Genes Dev 1995;9:639–49.
50. Gartel AL, Tyner AL. The role of the cyclin-dependent kinase inhibitor p21 in apoptosis. Mol Cancer Ther 2002;1:639–49.
51. Kwon YH, Jovanovic A, Serfas MS, Tyner AL. The Cdk inhibitor p21 is required for necrosis, but it inhibits apoptosis following toxin-induced liver injury. J Biol Chem 2003;278:30348–55.
52. Payne SR, Zhang S, Tsuchiya K, Moser R, Gurley KE, Longton G, De Boer J, Kemp CJ. p27kip1 deficiency impairs G2/M arrest in response to DNA damage, leading to an increase in genetic instability. Mol Cell Biol 2008;28:258–68.

The Journal of Immunology

Tyrosine Kinase 2 Plays Critical Roles in the Pathogenic CD4 T Cell Responses for the Development of Experimental Autoimmune Encephalomyelitis

Akiko Oyamada, Hiori Ikebe, Momoe Itsumi, Hirokazu Saiwai, Seiji Okada, Kazuya Shimoda, Yoichiro Iwakura, Keiichi I. Nakayama, Yukihide Iwamoto, Yasunobu Yoshikai and Hisakata Yamada

J. Immunol. 2009;183;7539-7546; originally published online Nov 16, 2009;
doi:10.4049/jimmunol.0902740
http://www.jimmunol.org/cgi/content/full/183/11/7539

The Journal of Immunology is published twice each month by The American Association of Immunologists, Inc., 9650 Rockville Pike, Bethesda, MD 20814-3994.

Print ISSN: 0022-1767 Online ISSN: 1550-6606.

Tyrosine Kinase 2 Plays Critical Roles in the Pathogenic CD4 T Cell Responses for the Development of Experimental Autoimmune Encephalomyelitis[1]

Akiko Oyamada,*‡ Hiori Ikebe,* Momoe Itsumi,* Hirokazu Saiwai,‡§ Seiji Okada,‡§ Kazuya Shimoda,† Yoichiro Iwakura,¶ Keiichi I. Nakayama,† Yukihide Iwamoto,‡ Yasunobu Yoshikai,* and Hisakata Yamada[2]*

Tyrosine kinase 2 (Tyk2), a member of the JAK family, is involved in IL-12- and IL-23-mediated signaling. In the present study, we examined the roles of Tyk2 in the development of myelin oligodendrocyte glycoprotein (MOG)-induced experimental autoimmune encephalomyelitis (EAE) by using Tyk2 knockout (KO) mice. In vitro differentiation of Th1 but not Th17 cells was severely impaired in Tyk2 KO CD4 T cells, although Tyk2 KO Th17 cells did not respond to IL-23. Tyk2 KO mice showed complete resistance against EAE with no infiltration of CD4 T cells in the spinal cord. Surprisingly, the number of MOG-specific Th17 cells in the periphery was comparable between KO and wild-type (WT) mice, whereas Th1 cells were greatly reduced in Tyk2 KO mice. Adoptive transfer of MOG-primed WT T cells induced EAE in Tyk2 KO recipients, indicating that Tyk2 in the environment was dispensable for the infiltration of effector T cells into the spinal cord. A reduced but significant number of Tyk2 KO T cells were detected in the spinal cord of mice with EAE, which had been reconstituted with bone marrow cells of WT and KO mice. Furthermore, MOG-immunized Tyk2 KO mice developed EAE after adoptive transfer of MOG-primed WT Th1 cells, which might trigger local inflammation that recruits Th17 cells. Taken together, these results indicate that Tyk2 is critically involved in the pathogenic CD4 T cell responses and thus could be a target molecule for the treatment of autoimmune diseases. *The Journal of Immunology,* **2009, 183: 7539–7546.**

Experimental autoimmune encephalomyelitis (EAE)[3] is an animal model of multiple sclerosis. EAE is induced by active immunization with myelin Ags or by adoptive transfer of myelin-specific CD4 T cells (1). Effector CD4 T cells in EAE have long been considered Th1 cells producing IFN-γ, but recent studies challenged this paradigm and demonstrated that a novel subset of helper CD4 T cells producing IL-17A, namely Th17 cells, were responsible for the development of EAE (2). The importance of Th17 cells in EAE was first suggested by a study using mice deficient for p19 subunit of IL-23 (3), which forms a heterodimer with the p40 subunit of IL-12 (4). IL-23p19- or p40-deficient mice, but not mice lacking p35, the unique subunit of IL-12, were totally resistant to the development of EAE despite a normal level of IFN-γ production by CD4 T cells. In contrast, IL-17A production by CD4 T cells was reduced in IL-23p19-deficient mice (5, 6). The importance of IL-17A in the pathogenesis of EAE was confirmed in studies using mice lacking IL-17A or mice treated with anti-IL-17A mAb, both of which were reported to develop a milder form of EAE (2, 7). Successful adoptive transfer of EAE by Th17 cells also indicates Th17 cells as the effectors of the disease (6). IL-23 was initially shown to induce differentiation of Th17 cells, but it is now generally accepted that the differentiation of Th17 cells depends on TGF-β and IL-6 and that IL-23 is instead involved in expansion, maintenance, and functional maturation of Th17 cells (8).

Although it has been shown that mice lacking IFN-γ or IFN-γR are susceptible to EAE (9–11), recent studies reevaluated the importance of Th1 responses in the pathogenesis of EAE. Kroenke et al. showed both IL-12-induced Th1 cells and IL-23-induced Th17 cells were able to induce EAE with distinct histopathology (12). It was also demonstrated that Th1 cells promote the entry of Th17 to the CNS in EAE (13). Consistently, IFN-γ induced expression of chemokines, which promoted T cell entry to the CNS (14). Therefore, both IL-12/Th1 and IL-23/Th17 axes seem to be involved in the pathogenesis of EAE, and signaling molecules involved in these axes might be the candidate therapeutic targets.

Tyrosine kinase 2 (Tyk2), a member of the JAK family, was originally identified as a signaling molecule of type I IFN receptor (15) and was later shown to be involved in IL-6 (16), IL-10 (17), and IL-12 signaling (18, 19). However, studies using mice genetically deficient for Tyk2 revealed different dependence of each cytokine signaling on Tyk2. Thus, Tyk2 is dispensable for IL-6- and IL-10-mediated signaling and plays only a small role in IFN-α

*Division of Host Defense, †Department of Molecular and Cellular Biology, Medical Institute of Bioregulation, and ‡Department of Orthopedic Surgery, §Research Superstar Program Stem Cell Unit, Graduate School of Medical Sciences, Kyushu University, Fukuoka, Japan; and ¶Center for Experimental Medicine, Institute of Medical Science, University of Tokyo, Tokyo, Japan

Received for publication August 19, 2009. Accepted for publication October 2, 2009.

The costs of publication of this article were defrayed in part by the payment of page charges. This article must therefore be hereby marked *advertisement* in accordance with 18 U.S.C. Section 1734 solely to indicate this fact.

[1] This work was supported in part by a grant from the Japan Rheumatism Foundation, a Grant-in-Aid for Scientific Research from the Japan Society for Promotion of Science, and by the Program of Founding Research Centers for Emerging and Reemerging Infectious Diseases launched as a project commissioned by the Ministry of Education, Culture, Sports, Science and Technology (MEXT), Japan.

[2] Address correspondence and reprint requests to Dr. Hisakata Yamada, Division of Host Defense, Medical Institute of Bioregulation, Kyushu University, 3-1-1 Maidashi, Higashi-ku, Fukuoka 812-8582, Japan. E-mail address: hisakata@bioreg.kyushu-u.ac.jp

[3] Abbreviations used in this paper: Tyk2, tyrosine kinase 2; dLN, draining lymph node; EAE, experimental autoimmune encephalomyelitis; KO, knockout; MOG, myelin oligodendrocyte glycoprotein; WT, wild type.

www.jimmunol.org/cgi/doi/10.4049/jimmunol.0902740

signaling (20, 21). On the other hand, IL-12-induced IFN-γ production by NK cells and activated T cells was highly dependent on Tyk2 (20–22). IL-23 and IL-12 commonly use the IL-12Rβ1 chain, which is associated with Tyk2, for their receptors (23). In fact, Tyk2 was shown to be involved in IL-23-induced STAT3 phosphorylation of activated T cells (24) and in IFN-γ production of dendritic cells (25). Furthermore, we recently reported that Tyk2 plays a crucial role in IL-23-induced IL-17A production by γδ T cells (26). However, the roles of Tyk2 in IL-23 signaling in Th17 cells remain unclear. The importance of Tyk2 in the in vivo differentiation of Ag-specific Th1 cells has also not been defined. Actually, we have observed a significant level of IFN-γ production by *Listeria monocytogenes*-specific CD8 T cells in Tyk2-deficient mice (27). In the present study, we examined the role of Tyk2 in Th1 and Th17 responses in a murine EAE model using Tyk2 knockout (KO) mice. We found that Tyk2-mediated signaling plays a critical role in the pathogenic CD4 T cell responses for the development of EAE.

Materials and Methods

Mice

C57BL/6 mice were purchased from Charles River Japan. Tyk2 KO and IL-17A KO mice were generated as previously described (20, 28). The mice were bred under specific pathogen-free conditions in our institute and have been backcrossed to C57BL/6 mice more than seven times. Six- to 10-wk-old mice were used for the experiments. The study design was approved by the Committee of Ethics on Animal Experiment at the Faculty of Medicine, Kyushu University. Experiments were conducted under the control of the Guidelines for Animal Experimentation.

Abs and flow cytometric analysis

FITC-conjugated anti-CD4 (RM4-5), anti-CD44 (IM7), anti-CD62L (MEL-14), anti-MHC class II (M5/114.15.2), anti-IFN-γ (XMG1.2), PE-conjugated anti-Ly5.1 (A20), anti-IFN-γ (XMG1.2), allophycocyanin-conjugated Ly5.2 (104), and Alexa Fluor 488-conjugated anti-mouse IL-17A (eBio17B7) mAbs were purchased from eBioscience. FITC-conjugated anti-CD11b (M1/70), PerCP-Cy5.5-labeled anti-CD4 (RM4-5), and allophycocyanin-conjugated anti-CD4 (CT-CD4) mAbs were purchased from BD Biosciences. For cell surface staining, a single-cell suspension was incubated with an optimal concentration of fluorescent mAb in HBSS with 0.5% FCS for 20 min at 4°C. Intracellular staining was performed using the BD Cytofix/Cytoperm kit (BD Biosciences) according to the manufacturer's instructions. Stained cells were run on a FACSCalibur flow cytometer (BD Biosciences). In some experiments, we added propidium iodide (1 μg/ml) to the cell suspension just before running on a flow cytometer to detect and exclude dead cells for the analysis. The data were analyzed using BD CellQuest software (BD Biosciences).

Cell purification

CD4 T cells were negatively selected by staining with anti-CD8 (2.43) and anti-I-A/E (M5/114.112.5) mAb for 20 min at 4°C, followed by incubation with Dynabeads sheep anti-rat IgG (Invitrogen) at 4°C. For further purification of naive CD4 T cells, CD4 T cells were stained with FITC-conjugated anti-CD62L mAb, followed by anti-FITC magnetic microbeads (Miltenyi Biotec). CD62L-positive cells were sorted by using an autoMACS (Miltenyi Biotec) according to the manufacturer's instructions. The purity of naive $CD44^{low}CD62L^{high}$CD4 T cells was >90%.

In vitro induction of Th1 and Th17 cells

Cell culture medium used was RPMI 1640 (Pure Chemicals) supplemented with 10% FBS (Cell Culture Technology), 100 U/ml penicillin, 100 mg/ml streptomycin, and 0.5 mM 2-ME. Purified naive CD4 T cells ($8–10 \times 10^5$ cells/ml in 48-well plates) were stimulated with 5 μg/ml plate-bound anti-CD3 (145-2C11) mAb and 1 μg/ml soluble anti-CD28 (37.51) mAb for 4 days. Th1 cells were induced by the addition of 1 ng/ml recombinant IL-12 (PeproTech) and 10 mg/ml anti-IL-4 (11B11) mAb to the culture. Th17 cells were induced by adding a combination of 20 ng/ml recombinant IL-6 (PeproTech) and 1 ng/ml human TGF-β1 (PeproTech) in the presence of 10 μg/ml anti-IFN-γ (XMG1.2) mAb and 10 μg/ml anti-IL-4 (11B11) mAb to the culture with or without 10 ng/ml recombinant IL-23 (R&D Systems). The amount of cytokines in the culture supernatant was measured by using ELISA kits (R&D Systems) according to the manufacturer's protocols. For intracellular staining, the cells were restimulated with 10 ng/ml PMA (Sigma-Aldrich) and 1 μg/ml ionomycin (Sigma-Aldrich) in the presence of 10 mg/ml brefeldin A (Sigma-Aldrich) for 5 h at 37°C.

Induction and assessment of EAE

Female mice at 7–10 wk of age were immunized s.c. on day 0 with 200 μg of myelin oligodendrocyte glycoprotein $(MOG)_{35–55}$ peptide emulsified in CFA containing 500 μg of *Mycobacterium tuberculosis* H37RA (Difco) and were injected i.p. on days 0 and 2 with 500 ng of pertussis toxin (List Biological Laboratories). Clinical scores were assigned according to the following criteria: 0, unaffected; 1, flaccid tail; 2, impaired righting reflex and/or gait; 3, partial hind limb paralysis; 4, total hind limb paralysis; 5, total hind limb paralysis with partial forelimb paralysis (29).

Measuring MOG-specific cytokine production

Purified CD4 T cells from draining lymph nodes (dLNs) were cultured with 10 μg/ml $MOG_{35–55}$ peptide and mitomycin C-treated wild-type (WT) splenocytes for 4 days. The amount of cytokines in the culture supernatants was measured by an ELISA assay. For intracellular cytokine staining, dLN or spinal cord cells were incubated for 4–5 h with 10 μg/ml $MOG_{35–55}$ peptide in the presence of 10 μg/ml brefeldin A at 37°C.

Histological analysis

Twenty-one days after EAE induction, mice were perfused transcardially with 4% paraformaldehyde in 0.1 M PBS. Spinal cords were extracted and embedded in OCT compound and sectioned horizontally at 14 mm on a cryostat. Sections were stained with H&E.

Isolation of mononuclear cells from spinal cords

Spinal cords were excised and cut into small pieces. They were dissociated for 1.5 h at 37°C by digestion with 100 U/ml collagenase D (Invitrogen) and 100 mg/ml DNase I (DN25; Sigma-Aldrich) in the cell culture medium. Dispersed cells were passed through a nylon mesh, placed onto 33% Percoll solution (Pharmacia), and centrifuged for 20 min at 2000 rpm. Cell pellets were resuspended in the culture medium and were used for analysis.

Adoptive transfer of EAE

Donor mice were immunized s.c. with 200 μg of $MOG_{35–55}$ peptide in CFA. Ten days later, dLN cells were cultured with 10 mg/ml $MOG_{35–55}$ peptide for 4 days. For preparation of Th1 cells, dLN cells from IL-17A KO mice were stimulated with $MOG_{35–55}$ peptide in the presence of 25 ng/ml IL-12 (PeproTech), 25 ng/ml IL-18 (Medical and Biological Laboratories) and 2 ng/ml IL-2 (PeproTech). Cells were harvested, washed with PBS, and injected i.v. to the recipient mice.

Generation of mixed bone marrow chimera mice

Bone marrow cells were prepared from WT (Ly5.1/5.1) mice and Tyk2 KO (Ly5.2/5.2) mice by flushing the femurs and tibias. RBCs were lysed with 0.83% ammonium chloride and the remaining mononuclear cells were resuspended in PBS for injection. Cells (5×10^6) from WT (Ly5.1/5.1) and Tyk2 KO (Ly5.2/5.2) mice were mixed and were injected i.v. into lethally irradiated WT recipient mice (Ly5.1/5.2). EAE was induced after confirming the reconstitution of CD4 T cells.

Statistics

Statistical significance was calculated by the Student's *t* test using Prism software (GraphPad Software). Differences with *p* values of <0.05 were considered statistically significant.

Results

Tyk2 is indispensable for the differentiation of naive CD4 T cells to Th1 cells but not to Th17 cells in vitro

To examine the involvement of Tyk2 in cytokine signaling for the differentiation of naive CD4 T cells to Th1 or Th17 cells, $CD62L^{high}CD44^{low}$ CD4 T cells were purified from Tyk2 KO or WT mice and were cultured in vitro with plate-bound anti-CD3 and soluble anti-CD28 for 4 days under Th1- or Th17-polarizing condition (Fig. 1). Differentiation into Th1 cells was severely impaired in Tyk2 KO CD4 T cells, which is consistent with a previous finding that Tyk2 was critical to IL-12 signaling (20, 21). On the other hand, Tyk2 KO CD4 T cells differentiated into Th17 cells

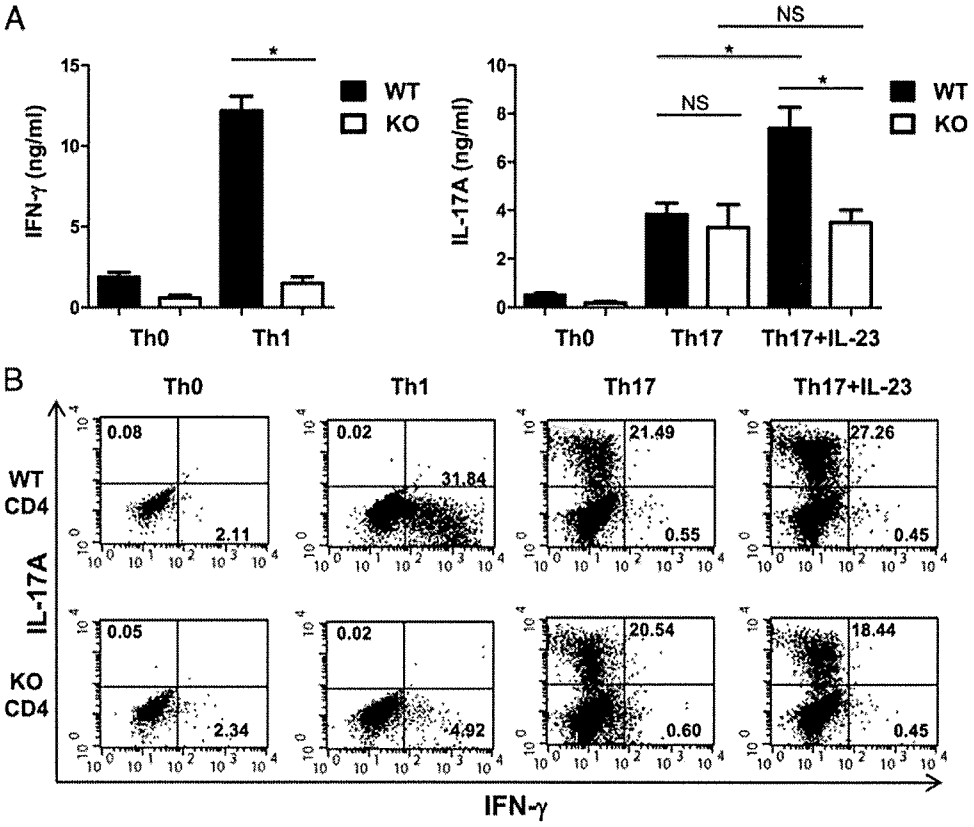

FIGURE 1. Tyk2 was indispensable for in vitro differentiation of naive CD4 T cells to Th1 cells but not to Th17 cells. CD62L^{high}CD44^{low}CD4 T cells from WT and Tyk2 KO mice were cultured with plate-bound anti-CD3 mAb and soluble anti-CD28 mAb for 4 days under Th1-polarizing conditions (IL-12 and anti-IL-4 mAb) or Th17-polarizing conditions (TGF-β, IL-6, and anti-IFN-γ and anti-IL-4 mAbs) with or without IL-23. *A*, The amount IFN-γ (*left*) and IL-17A (*right*) in the culture supernatants was measured by ELISA. *B*, Cultured cells were restimulated with PMA and ionomycin in the presence of brefeldin A for 5 h and were tested for intracellular staining of IFN-γ and IL-17A. The data are representative of four independent experiments. Error bars represent mean ± SEM. *, $p <$ 0.05.

as efficiently as did WT CD4 T cells, indicating that Tyk2 is dispensable for IL-6-signaling required for Th17 differentiation. Notably, Th17 cells generated from Tyk2 KO CD4 T cells did not expand in response to IL-23. Therefore, Tyk2 plays a critical role in signal transduction from IL-12 and IL-23 receptors in Th1 and Th17 cells, respectively.

Tyk2 is indispensable for the development of EAE and induction of IFN-γ but not IL-17A production in vivo

We next examined the roles of Tyk2 in the in vivo differentiation of Th1 and Th17 cells in a murine EAE model. EAE was induced by immunization of MOG_{35-55} peptide emulsified with CFA, which was followed by i.p. injection with pertussis toxin on days 0 and 2. WT mice started to develop EAE 10 days after immunization and reached the peak score at ~3 wk with 100% incidence (Fig. 2*A*). In contrast, Tyk2 KO mice never showed any disease symptoms, including loss of body weight (Fig. 2, *A* and *B*). Thus, Tyk2 was indispensable for the development of EAE. To examine cytokine production by MOG-specific CD4 T cells, dLNs were harvested 10 days after immunization and were stimulated with MOG_{35-55}. Consistent with the results of the in vitro differentiation experiments, CD4 T cells in Tyk2 KO mice produced nearly an undetectable level of IFN-γ and a reduced but significant level of IL-17A in response to MOG_{35-55} (Fig. 2*C*). There were no differences in MOG_{35-55}-specific IL-10, IL-4, and TNF-α production by CD4 T cells in Tyk2 KO and WT mice (data not shown). An equivalent number of CD25$^+$FoxP3 regulatory CD4 T cells were detected in WT and Tyk2 KO mice (data not shown). These results suggest that Tyk2 is also critical to the development of Th1 but not Th17 cells in vivo, and therefore the EAE resistance of

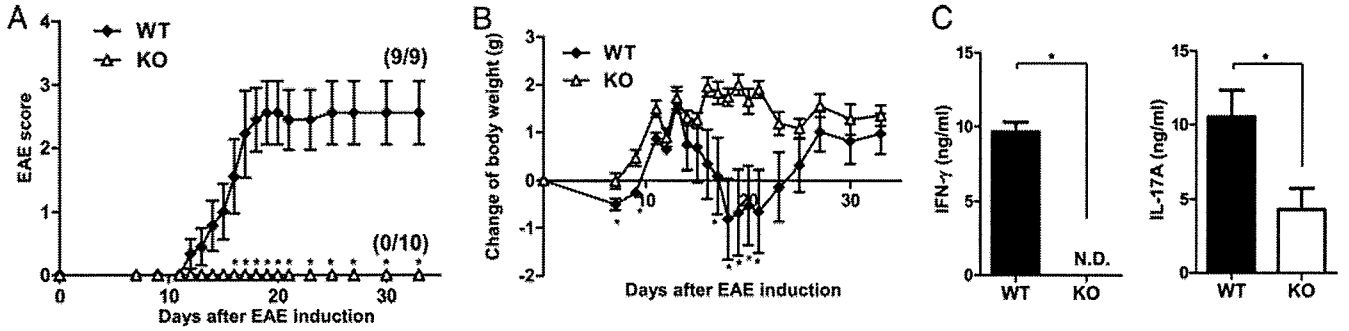

FIGURE 2. Tyk2 was indispensable for the development of EAE but not for IL-17A production by CD4 T cells in vivo. EAE was induced by immunization with MOG_{35-55} peptide emulsified with CFA, followed by i.p. injection with pertussis toxin on days 0 and 2. *A*, EAE clinical score and (*B*) the changes of body weight from the time of immunization are shown. Numbers in parentheses show disease incidence. Data are representative of three independent experiments. *C*, CD4 T cells were purified from dLNs 10 days after immunization (n = 3) and were stimulated with MOG_{35-55} for 4 days. Amount of IFN-γ (*left*) and IL-17A (*right*) in the culture supernatants was measured by ELISA. Data are representative of four separate experiments. Error bars represent mean ± SEM. *, $p < 0.05$ between WT and Tyk2 KO mice. N.D., Not detected.

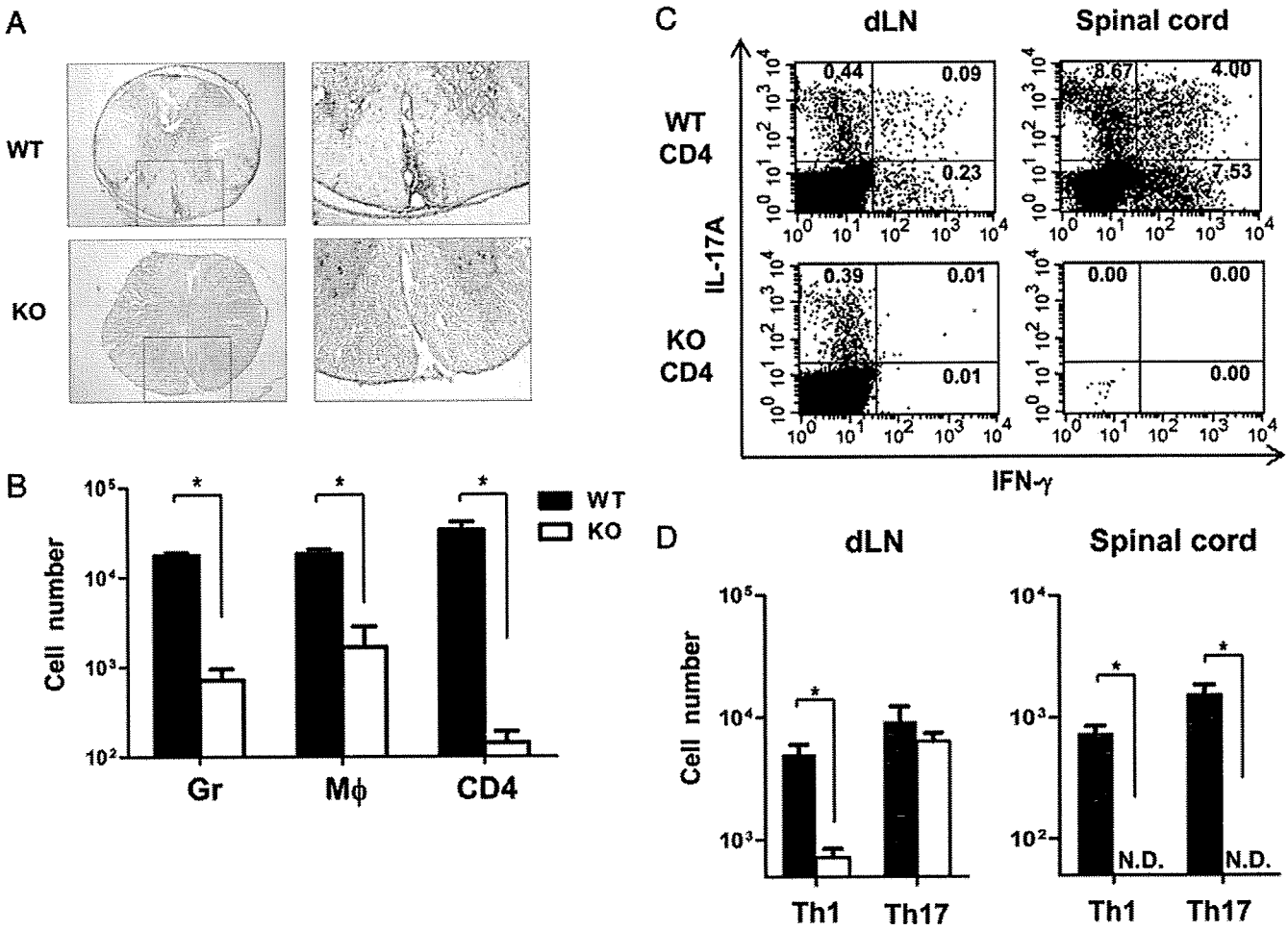

FIGURE 3. Absence of CD4 T cells in the spinal cord of Tyk2 KO mice. *A*, Histological analysis by H&E staining of spinal cords was performed 21 days after immunization. Right panels show the magnified view of the area within the square in left panels. Magnification, *left*, ×40; right, ×100. *B*, Absolute numbers of MHC class $II^-Gr\text{-}1^+$ cells (granulocytes, Gr), MHC class II^+CD11b^+ cells (macrophages, Mϕ), and CD4 T cells in the spinal cord of WT and Tyk2 KO mice 21 days after immunization were calculated by using flow cytometry. *C*, Lymphocytes from dLNs and the spinal cord were stimulated with MOG_{35-55} peptide for 5 h in the presence of brefeldin A. Intracellular staining of IFN-γ and IL-17A was performed. *D*, Absolute numbers of Th1 and Th17 cells in dLNs and the spinal cord were calculated. Error bars represent mean ± SEM. *, $p < 0.05$.

Tyk2 KO mice might not be simply attributed to the defective induction of Th17 responses.

Defective infiltration of CD4 T cells in the spinal cord of Tyk2 KO mice despite abundance of Th17 cells in the periphery

To elucidate the mechanism for the resistance of Tyk2 KO mice in the development of EAE, histological analysis of the spinal cord was performed 21 days after EAE induction (Fig. 3*A*). Infiltration of lymphocytes was clearly detected in the spinal cord of WT mice, whereas no cellular infiltration was found in the spinal cord of Tyk2 KO mice. The extent of cellular infiltration in the spinal cord was quantified by flow cytometric analysis. The number of neutrophils and macrophages was greatly reduced in Tyk2-deficient mice. The number of CD4 T cells in Tyk2 KO mice was also much lower than that of WT mice and was comparable to that of naive normal mice (Fig. 3*B*, data not shown). Intracellular staining of cytokines revealed that CD4 T cells in the spinal cord of WT mice included both Th1 and Th17 cells specific for the MOG peptide (Fig. 3*C*). Surprisingly, in the dLN, the number of CD4 T cells, including MOG_{35-55}-specific Th17 cells, was comparable between Tyk2-deficient mice and WT mice (Fig. 3, *C* and *D*). Therefore, it was suggested that an impaired recruitment of effector CD4 T cells to the spinal cord was responsible for the disease resistance of Tyk2-deficient mice.

Expression of Tyk2 in the environment is dispensable for the infiltration of effector CD4 T cells into the spinal cord

These observations raised a possibility that Tyk2 in the environment regulates the infiltration of Th17 cells in the spinal cord. Therefore, we next examined adoptively induced EAE using Tyk2 KO mice. We found that naive Tyk2 KO recipients developed EAE after receiving MOG_{35-55}-primed WT CD4 T cells (Fig. 4). The disease severity of Tyk2 KO mice was similar to the level of WT mice. In contrast, MOG peptide-primed CD4 T cells from Tyk2 KO mice, which contain a significant number of Th17 cells, did not induce EAE in WT recipients. Therefore, the expression of Tyk2 in CD4 T cells, but not in the environment, was indispensable for the infiltration of effector CD4 T cells into the spinal cord.

A significant but reduced infiltration of Tyk2 KO CD4 T cells into the spinal cord of mice developing EAE

To elucidate the roles of Tyk2 in the environment and in CD4 T cells from the induction stage of EAE, we performed mixed bone marrow chimera experiments by using Ly5.1-congenic C57BL/6 mice. Recipient WT mice (Ly5.1/5.2) were lethally irradiated and transferred with a mixture of bone marrow cells from WT (Ly5.1/5.1) and Tyk2 KO (Ly5.2/5.2) mice. After confirming the reconstitution of CD4 T cells, the mice were immunized with MOG_{35-55}.

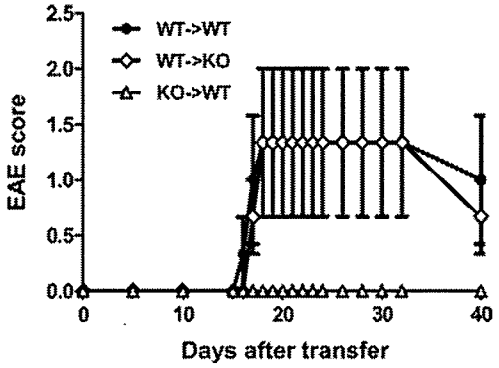

FIGURE 4. Tyk2 KO mice were susceptible for adoptively transferred EAE. WT and Tyk2 KO mice were immunized with MOG_{35-55} peptide. Ten days later, lymphocytes harvested from dLNs were restimulated in vitro with MOG_{35-55} for 4 days and were transferred into naive WT or Tyk2 KO mice (10×10^6 cells/recipient). Data are representative of two independent experiments. Error bars represent mean ± SEM.

All the mixed bone marrow chimera mice developed EAE, suggesting no dominant disease-suppressing activity of Tyk2 KO bone marrow-derived cells (Fig. 5*A*). On day 21 after induction of EAE, the ratio of WT (Ly5.1/5.1) to Tyk2 KO (Ly5.2/5.2) cells, including CD4 T cells in dLNs, was >2-fold for unknown reasons (Fig. 5*B*, data not shown). Importantly, Tyk2 KO CD4 T cells were also detected in the spinal cord of the bone marrow chimera mice, although the proportion was lower than WT CD4 T cells (Fig. 5*B*). Additionally, absolute numbers of MOG-specific Th17 cells as well as Th1 cells in the spinal cord were much lower in Tyk2 KO T cells than in WT T cells (Fig. 5*C*), indicating an importance of Tyk2 signaling in CD4 T cells for their differentiation into effector cells capable of infiltrating into the spinal cord. Nevertheless, the number of Tyk2-deficient Th17 cells in the spinal cord was increased compared with unmanipulated Tyk2 KO mice that were similarly immunized with MOG_{35-55} (Fig. 3*D*). Thus, it was also suggested either that Tyk2-deficient Th17 cells generated in a Tyk2-sufficient environment have some capacity to infiltrate into the spinal cord or that Tyk2-deficient T cells could infiltrate into the spinal cord when local inflammation was provoked by Tyk2-sufficient CD4 T cells. To verify these possibilities, we set up the following experiment. WT (Ly5.1/5.1) and Tyk2-deficient (Ly5.2/5.2) mice were immunized with MOG_{35-55} peptide. dLN cells from each group were harvested and restimulated with the peptide for 4 days, and a mixture of these effector CD4 T cells was transferred into WT (Ly5.1/5.2) mice that had been immunized with MOG and were developing EAE (Fig. 6*A*). Seven days after transfer, Tyk2 KO CD4 T cells were clearly detected in the spinal cord, although here again the number of Tyk2 KO cells was lower than WT cells (Fig. 6*B*). Therefore, even Tyk2-deficient CD4 T cells primed in a Tyk2-deficient environment could infiltrate into the spinal cord, although with reduced efficiency, once local inflammation was provoked.

EAE could be induced in Tyk2 KO mice by supplementing Th1 cells

Since Th1 cells were reported to facilitate local infiltration of Th17 cells (13), a defective Th1 response in Tyk2 KO mice might be involved in the defective CD4 T cell infiltration in the spinal cord and also in the resistance against EAE. To test this possibility, we transferred MOG-specific Th1 cells generated from IL-17A KO mice into MOG_{35-55}-immunized Tyk2 KO mice (Fig. 7*A*). We transferred a relatively small number of Th1 cells, which by themselves did not induce EAE in naive WT recipient mice. However,

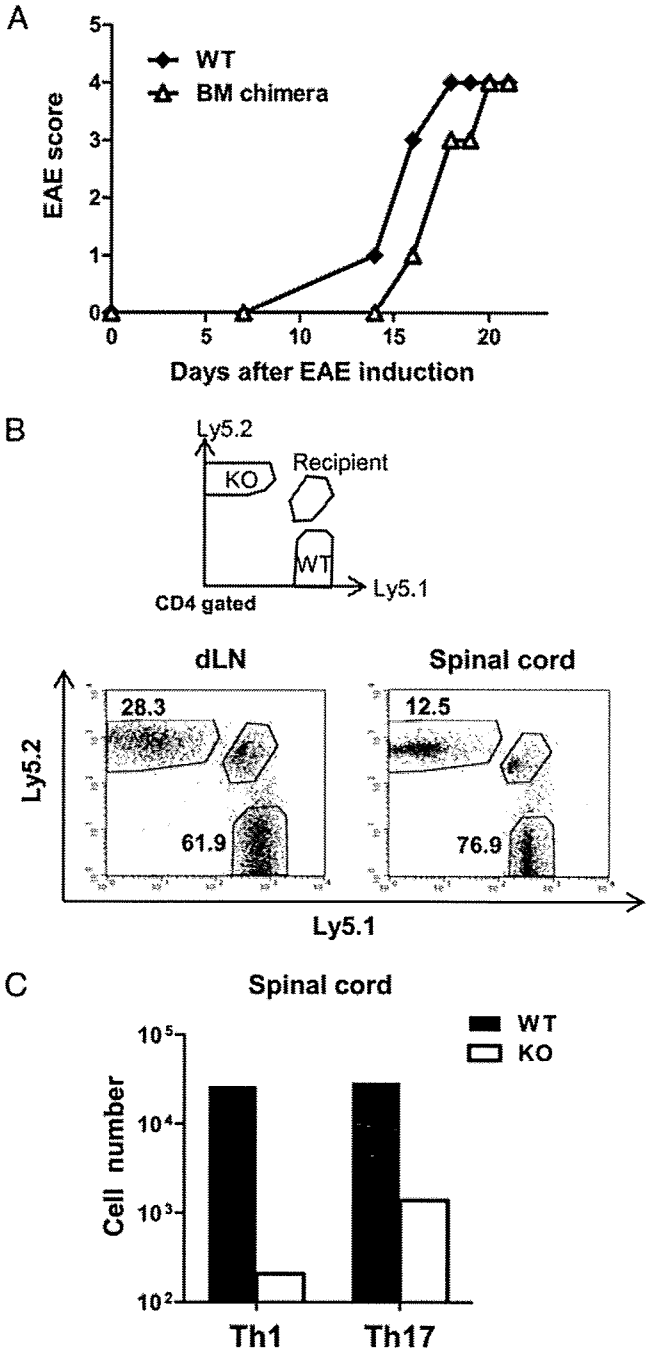

FIGURE 5. Tyk2-deficient CD4 T cells in mixed bone marrow chimera mice were able to infiltrate in the spinal cord with EAE. WT mice expressing Ly5.1/5.2 were lethally irradiated and reconstituted with a mixture of bone marrow cells from WT mice (Ly5.1/5.1) and Tyk2 KO mice (Ly5.2/5.2). EAE was induced in the mixed bone marrow chimera mice. *A*, EAE clinical scores of unmanipulated WT mice and the chimera mice are shown. *B*, On day 21, chimerism in dLNs and the spinal cord was examined by flow cytometry. Representative dot plots are shown after gating on $CD4^+$ cells. *C*, Absolute numbers of Th1 and Th17 cells in the spinal cords were calculated after flow cytometric analysis of intracellular staining. Data are representative of two separate experiments.

such a small number of MOG_{35-55}-specific Th1 cells induced EAE in MOG_{35-55}-immunized Tyk2 KO mice (Fig. 7*B*). Therefore, it was suggested that the lack of Th1 cells in Tyk2 KO mice might also be involved in their resistance against EAE, and that MOG_{35-55}-primed T cells in Tyk2 KO mice contributed to the development of EAE.